Royal Netherlands Institute for Sea Research

Jones, E.M.; Hoppema, M.; Bakker, K.; de Baar, H.J.W. (2021). Calcium carbonate saturation states along the West Antarctic Peninsula. *Antarctic Science 33(6)*: 575-595.
DOI: 10.1017/ s0954102021000456

Published version: https://dx.doi.org/10.1017/s0954102021000456

NIOZ Repository: http://imis.nioz.nl/imis.php?module=ref&refid=347206

[Article begins on next page]

[Running heads – even pages: Elizabeth M. Jones *et al.*; odd pages: Calcium carbonate saturation states along the West Antarctic Peninsula

Author email: *elizabeth.jones@hi.no*

Please note: Colour figs]

Calcium carbonate saturation states along the West Antarctic Peninsula

ELIZABETH M. JONES[1,2], MARIO HOPPEMA[3], KAREL BAKKER[4,5] AND HEIN J.W. DE BAAR[2,6]

[1]*Institute of Marine Research, Fram Centre, Hjalmar Johansens gate 14, 9007 Tromsø, Norway*

[2]*NIOZ, Royal Netherlands Institute for Sea Research, Den Burg, The Netherlands*

[3]*Alfred Wegener Institute Helmholtz Centre for Polar and Marine Research, Climate Sciences Department, Postfach 120161, 27515 Bremerhaven, Germany*

[4]*NIOZ, Royal Netherlands Institute for Sea Research, Department of Ocean Systems* (*OCS*)*, Den Burg, The Netherlands*

[5]*Utrecht University, PO Box 59, Den Burg 1790 AB, The Netherlands*

[6]*Ocean Ecosystems, University of Groningen, Nijenborgh 7, 9747 AG, Groningen, The Netherlands*

elizabeth.jones@hi.no

Elizabeth M. Jones ORCID number: 0000-0001-7660-0238

Mario Hoppema ORCID number: 0000-0002-2326-619X

Hein J.W. de Baar ORCID number: 0000-0002-8750-7079

Abstract: The waters along the West Antarctic Peninsula (WAP) have experienced warming and increased freshwater inputs from melting sea ice and glaciers in recent decades. Challenges exist in understanding the consequences of these changes on the inorganic carbon system in this ecologically important and highly productive ecosystem. Distributions of dissolved inorganic carbon (C_T), total alkalinity (A_T) and nutrients revealed key physical, biological and biogeochemical controls of the calcium carbonate saturation state ($\Omega_{aragonite}$) in different water masses across the WAP shelf during the summer. Biological production in spring and summer dominated changes in surface water $\Omega_{aragonite}$ ($\Delta\Omega_{aragonite}$ up to +1.39; ~90%) relative to underlying Winter Water. Sea-ice and glacial meltwater constituted a minor source of A_T that increased surface water $\Omega_{aragonite}$ ($\Delta\Omega_{aragonite}$ up to +0.07; ~13%). Remineralization of organic matter and an influx of carbon-rich brines led to cross-shelf decreases in $\Omega_{aragonite}$ in Winter Water and Circumpolar Deep Water. A strong biological carbon pump over the shelf created $\Omega_{aragonite}$ oversaturation in surface waters and suppression of $\Omega_{aragonite}$ in subsurface waters. Undersaturation of aragonite occurred at < ~1000 m. Ongoing changes along the WAP will impact the biologically driven and meltwater-driven processes that influence the vulnerability of shelf waters to calcium carbonate undersaturation in the future.

Received 23 October 2020, accepted 19 August 2021

Key words: alkalinity, aragonite, Circumpolar Deep Water, inorganic carbon system, meltwater

Introduction

The waters off the West Antarctic Peninsula (WAP) support some of the highest rates of phytoplankton primary production in the whole of the Southern Ocean and play a large role in biogeochemical cycling (Arrigo *et al.* 2008, Clarke *et al.* 2008). The marine environment of the WAP is strongly influenced by the offshore Antarctic Circumpolar Current (ACC; Fig. 1) that impacts the western shelf with intrusions of relatively warm upper Circumpolar Deep Water (uCDW; Fig. 2) across the shelf-break (Martinson *et al.* 2008). Along the shelf, glacial meltwater and melting sea ice stratify the water column to form relatively fresh Antarctic Surface Water (AASW) in the summer mixed layer overlying the permanent pycnocline that extends to the nutrient-rich and carbon-rich uCDW (Meredith *et al.* 2013). The AASW caps the cold and saline remnant of the winter mixed layer, called the Winter Water, which is identified by a minimum in potential temperature (Venables *et al.* 2013). The Winter Water in spring and summer reflects the (biogeochemical) signatures of the surface layer of the preceding winter; however, some modification through advection, mixing and remineralization of organic matter is probable. Mixing of uCDW with overlying AASW and Winter Water forms modified CDW (mCDW) over the shelf, which is channelled into the coastal zone through numerous glacially eroded canyons (Smith *et al.* 1999, Martinson *et al.* 2008). Deep convective mixing during winter, following brine rejection from sea ice, cools and increases the salt content of the Winter Water (Venables *et al.* 2013).

The WAP shelf is an ecologically important region (Clarke *et al.* 2008, Ducklow *et al.* 2013) with high primary productivity (Schofield *et al.* 2017) driving substantial oceanic uptake of carbon dioxide (CO_2) from the atmosphere (Arrigo *et al.* 2008, Brown *et al.* 2019). The inorganic carbon system along the WAP is strongly regulated by meltwater inputs, primary production and respiration, sea-ice processes, mixing of different water masses and carbonate mineral formation and dissolution (e.g. Hauri *et al.* 2015, Tortell *et al.* 2015). The seasonal retreat of the ice pack exposes surface waters to increased light levels where freshwater from melting glaciers, sea ice and snow stratifies the upper ocean across the WAP shelf (Meredith *et al.* 2013, Venables *et al.* 2013). Release of micronutrients, such as iron, and seeding by sea-ice algae promote the onset of phytoplankton blooms (Clarke *et al.* 2008, Vernet *et al.* 2008, Schofield *et al.* 2017), driving intense uptake of inorganic carbon and nutrients. Phytoplankton blooms during spring and summer create hotspots of biological production and drawdown of atmospheric CO_2 along the WAP shelf (Hauri *et al.* 2015, Tortell *et al.* 2015, Kerr *et al.* 2018). Diatoms are key species in summertime phytoplankton communities, removing silicic acid (silicate) from the surface layer, and the subsequent export and dissolution of biogenic silica in subsurface waters is an important pathway in nutrient cycling in the region (Schofield *et al.* 2017, Henley *et al.* 2018, Tréguer *et al.* 2018). Coastal and shelf waters are typically iron-replete due to their proximity to glacial and sedimentary sources of iron, in addition to oceanic iron supply with transient periods of iron limitation during the growing season (Dinniman *et al.* 2020 and references cited therein). Macronutrients are replete over the WAP shelf, apart from exceptional episodic depletion in the surface layer that rarely occurs (and may not be subsequently captured and measured) following intense uptake in the spring and summer blooms (Henley *et al.* 2018). Remineralization of exported organic matter from productive surface waters and enrichment of the inorganic carbon and nutrient pools in subsurface waters is pronounced following the highly productive summer period (Jones *et al.* 2017, Henley *et al.* 2018). Phytoplankton productivity decreases offshore as strong winds enhance mixing, removing phytoplankton from the surface layer, and, remote from topographical features, the supply and concentrations of iron can be limiting (e.g. Vernet *et al.* 2008, Trimborn *et al.* 2015). Episodic intrusions of CDW enrich the surface layer with inorganic carbon and, in the absence of efficient biological carbon drawdown, drive supersaturation of CO_2 with respect to the atmosphere (Hauri *et al.* 2015, Jones *et al.* 2017, Kerr *et al.* 2018).

Sea-ice processes influence carbon cycling through the formation and dissolution of the abiotic calcium carbonate mineral ikaite ($CaCO_3 \cdot 6H_2O$) (Rysgaard *et al.* 2007, Dieckmann *et al.* 2008). These processes lead to shifts in dissolved inorganic carbon (C_T; Eq. (1)) and total alkalinity (A_T; Eq. (2)):

$$C_T = [H_2CO_3^*] + [HCO_3^-] + [CO_3^{2-}] \quad (1)$$

$$A_T = [HCO_3^-] + 2[CO_3^{2-}] + [B(OH)_4^-] + [OH^-] - [H^+] + \text{proton acceptors - proton donors} \quad (2)$$

where $[HCO_3^-]$ and $[CO_3^{2-}]$ are concentrations of bicarbonate and carbonate, respectively, and $[H_2CO_3^*]$ comprises the concentrations of carbonic acid (H_2CO_3) and aqueous CO_2. The H_2CO_3 content is negligible for practical purposes. The A_T is dominated by $[HCO_3^-]$ and $[CO_3^{2-}]$ representing ~76% and ~19%, respectively (when pH ≈ 8.1), and describes the capacity of seawater to buffer against acidic inputs (e.g. CO_2) (Dickson 1981, Sarmiento & Gruber 2006). Ikaite crystals precipitate during sea-ice formation in autumn and winter where, due to the incorporation of calcium ions (Ca^{2+}) and CO_3^{2-}, the A_T decreases by 2 for each ikaite molecule that is formed. These processes partition A_T within sea ice relative to the surrounding seawater as ikaite is retained within the brine channels and pockets in the sea ice (Dieckmann *et al.* 2008) and the CO_2-rich brines are rejected and increase the C_T content of the ice-covered upper ocean (Rysgaard *et al.* 2007). During sea-ice melt in spring and summer, meltwater inputs dilute A_T, hence lowering the buffer capacity of seawater; however, ikaite dissolution creates a small source of A_T that slightly counteracts the dilution effects (Hauri *et al.* 2015, Jones *et al.* 2017, Legge *et al.* 2017).

Since the Industrial Revolution, the concentration of CO_2 in the atmosphere has increased from ~280 to ~410 matm in 2019 (https://www.esrl.noaa.gov/gmd/ccgg/trends/gl_data.html), leading to invasion of atmospheric CO_2 into the ocean through the solubility carbon pump. Increased oceanic uptake of CO_2 increases the C_T in surface waters, resulting in increases in hydrogen ion concentrations ($[H^+]$), reductions in $[CO_3^{2-}]$ and lowering of seawater pH at a rate of ~0.02 pH units per decade since the late 1980s (https://www.ipcc.ch/srocc/chapter/chapter-5). Declining pH and $[CO_3^{2-}]$ are commonly referred to as ocean acidification (Feely *et al.* 2004, Orr *et al.* 2005); however, the seawater will remain basic, albeit a bit less basic (i.e. pH < 8.1–8.2), rather than becoming acidic. The lowering of $[CO_3^{2-}]$ leads to a reduction in the calcium carbonate ($CaCO_3$) saturation states of the biominerals aragonite ($\Omega_{aragonite}$) and calcite ($\Omega_{calcite}$), defined for aragonite as follows:

$$\Omega_{aragonite} = ([Ca^{2+}]_{sw} \times [CO_3^{2-}]_{sw})/K^*_{SP\ aragonite} \quad (3)$$

where $[Ca^{2+}]_{sw}$ and $[CO_3^{2-}]_{sw}$ are the concentrations in ambient seawater and $K^*_{SP\ aragonite}$ is the solubility product of aragonite as a function of salinity, temperature and pressure (Broecker & Peng 1982, Sarmiento & Gruber 2006). The biotic $CaCO_3$ minerals aragonite and calcite and the abiotic $CaCO_3$ mineral ikaite have their own solubility properties (as a function of seawater temperature, salinity and pressure). Ikaite is extremely unstable and can only exist in crystalline form at low temperatures and high salinities (Dieckmann *et al.* 2008 and references cited therein). Aragonite is the less stable biomineral found in marine calcifiers due to its comparatively higher solubility relative to calcite. As such, aragonite is most vulnerable to dissolution and seawater is undersaturated when $\Omega_{aragonite} < 1$, whereby conditions can become energetically costly and potentially even corrosive for calcifiers (Feely *et al.* 2004, Orr *et al.* 2005).

The WAP marine environment has been routinely monitored through the US Palmer Long-Term Ecological Research (PAL-LTER) programme (Ducklow *et al.* 2013) and the British Antarctic Survey Rothera Time Series (RaTS) (Clark *et al.* 2008). High spatial variability and seasonality in inorganic carbon cycling is superimposed on decadal variations in ocean warming, intrusions of carbon-rich CDW onto the shelf, glacial melting and shortening of the sea-ice season (e.g. Vaughan *et al.* 2003, Martinson *et*

al. 2008). Increased and more southern upwelling of CDW in response to the El Niño Southern Oscillation and Southern Annular Mode (Hall & Visbeck 2002, Stammerjohn *et al.* 2008) further influences the seasonal sea-ice cover and oceanographic conditions along the WAP. Decadal enrichment of C_T and lowering of pH have already been reported in surface and subsurface waters along the WAP (Hauri *et al.* 2015, Kerr *et al.* 2018), and aragonite undersaturation has been found in the shallower water column closer to the coast (Jones *et al.* 2017). Encroaching $CaCO_3$ undersaturation may have impacts on pelagic and benthic calcifiers such as pteropods that are important links between trophic levels and key contributors to organic and inorganic carbon cycling along the WAP (Feely *et al.* 2004, Bednaršek *et al.* 2012, Thibodeau *et al.* 2019). In addition, shifts in the inorganic carbon system may affect phytoplankton productivity and community composition (Trimborn *et al.* 2015 and references cited therein), which control the efficiency of atmospheric CO_2 uptake, export of organic carbon and biogeochemical cycling (e.g. Arrigo *et al.* 2008). Understanding the collective effects of these processes that drive changes in calcium carbonate saturation states is key to better assessing future trends in carbon cycling and potential impacts to the Antarctic ecosystem (Hauri *et al.* 2015, Kerr *et al.* 2018). This study, presenting new water column data along and across the WAP continental shelf, complements those from earlier campaigns with new insights into the role of 1) phytoplankton production, 2) the release of sea-ice and glacial meltwater containing dissolved minerals and 3) freshwater dilution and mixing of CDW, all of which drive spatial variability in calcium carbonate saturation in different water masses across the WAP shelf in summer.

Methods

Sampling and hydrography

Water samples were collected and hydrographic measurements were carried out in summer (9–31 January 2011) along the WAP (Fig. 1) during expedition ANT-XXVII/2 on board FS *Polarstern*. A total of 19 stations were occupied along three transects extending from the open ocean waters of the ACC (offshore, depth > 1000 m) to nearshore and coastal waters (shelf, depth < 750 m) of the WAP (Fig. 2). The area extended from 65°W (west of Anvers Island) to 75°W (west of Adelaide Island) and 63°S to 67°S. Depth profiles of potential temperature and salinity were obtained using a conductivity-temperature-depth (CTD) instrument (SBE 9/11plus) mounted onto a Seabird Carousel Water Sampler type SBE32 equipped with 12 l Ocean Test Equipment bottles type SBE improved Model 110.

The definition of the mixed-layer depth (MLD) is taken as the depth where the potential density exceeds 0.05 kg m^{-3} relative to 10 m depth (Venables *et al.* 2013). The depth of the potential temperature minimum (θ_{min}) is taken to represent the core of the Winter Water (remnant of the winter mixed layer). Salinity is reported on the practical salinity scale. Hydrographic data are available in the PANGAEA database (https://doi.org/10.1594/PANGAEA.772244). Ocean Data View 4 (http://odv.awi.de) was used for data visualization.

Inorganic carbon system

Seawater samples for C_T and A_T were drawn from the Water Sampler bottles into 500 ml borosilicate glass bottles and analysed within 20 h on a VINDTA 3C instrument (Marianda, Kiel, Germany). Analyses for C_T were made through coulometric determination and A_T determination was carried out by automated potentiometric titration, following standard procedures (Dickson *et al.* 2007). Certified Reference Materials (CRM, batches 100 and 105) supplied by A.G. Dickson (Scripps Institution of Oceanography) were analysed to calibrate the measurements; the precision of these analyses was 1.0 μmol kg^{-1} for C_T and 1.5 μmol kg^{-1} for A_T. The ranges of A_T (2342–2357 μmol kg^{-1}) and C_T (2253–2277 μmol kg^{-1}) in mCDW in this study are consistent

with those previously reported for the wider WAP region (2350 µmol A_T kg^{-1} and 2253 µmol C_T kg^{-1}; Hauri *et al.* 2015) and coastal waters on Adelaide Island (~2340 µmol A_T kg^{-1} and ~2260 µmol C_T kg^{-1}; Jones *et al.* 2017). The deep water observations correspond very well to previous measurements from the PAL-LTER 1998–2012 cruises (C_T = 2261 ± 4 µmol kg^{-1}; A_T = 2365 ± 7 µmol kg^{-1}), World Ocean Circulation Experiment (WOCE) and Climate and Ocean - Variability, Predictability, and Change (CLIVAR) cruises (1992, 2006, 2009, 2011) and accompanying calculated variables (C_T = 2262 ± 3 µmol kg^{-1}; A_T = 2366 ± 9 µmol kg^{-1}), as reported in Hauri *et al.* (2015).

The $\Omega_{aragonite}$ (Eq. (3)) and $\Omega_{calcite}$ were calculated from C_T (Eq. (1)), A_T (Eq. (2)) and *in situ* temperature, salinity, pressure and concentrations of phosphate and silicic acid using the *CO2SYS* program (van Heuven *et al.* 2011). The carbonic acid dissociation constants K_1 and K_2 (Eqs (4) & (5)) determined in natural seawater by Mehrbach *et al.* (1973) as refitted by Dickson & Millero (1987) were selected. The constants K_1 and K_2 are functions of salinity (*S*) and temperature (*T*) in natural seawater and are derived from the equilibrium relationships between the inorganic carbon species (Eq. (1)):

$$K_1 = [H^+][HCO_3^-]/[H_2CO_3^*] \quad (4)$$

and

$$K_2 = [H^+][CO_3^{2-}]/[HCO_3^-] \quad (5)$$

These constants were determined for $19 \leq S \leq 43$ and $2°C \leq T \leq 35°C$ and have been used in previous studies in the Southern Ocean and WAP regions where temperatures are frequently < 0°C (e.g. Bednaršek *et al.* 2012, Hauri *et al.* 2015, Jones *et al.* 2017). More recent determinations of K_1 and K_2 in natural seawater by Mojica Prieto & Millero (2002) have been shown to be in excellent agreement with the values of Mehrbach *et al.* (1973), where the combined data have been fitted as functions of temperature (0–45°C) and salinity (5–42) by Mojica Prieto & Millero (2002). The values of $\Omega_{aragonite}$ and $\Omega_{calcite}$ are used as indicators for changes in carbonate chemistry in relation to calcium carbonate saturation states and potential ocean acidification. When $\Omega_{aragonite} < 1$, the seawater is undersaturated with respect to aragonite, such that aragonite minerals become sensitive to dissolution and seawater becomes corrosive to organisms that produce aragonitic shells and skeletons (Feely *et al.* 2004, Orr *et al.* 2005). The $\Omega_{calcite}$ remained positive (seawater was oversaturated with respect to calcite) in the upper ~2000 m of the water column. Therefore, this study is focused on $\Omega_{aragonite}$ and its changes ($\Delta\Omega_{aragonite}$) with respect to acidification in the contemporary and future marine environment along the WAP. The corresponding values for calcite ($\Omega_{calcite}$) and its changes ($\Delta\Omega_{calcite}$) are included as references.

Inorganic nutrients

For inorganic macronutrients silicic acid ($Si(OH)_4$, commonly referred to as silicate), phosphate (PO_4), nitrate + nitrite (NO_3 + NO_2) and nitrite (NO_2), seawater was transferred from sample bottles into pre-rinsed 5 ml polyethylene vials and analysed with a Technicon TRAACS 800 Auto-analyzer. A freshly diluted home-made mixed nutrient standard containing $Si(OH)_4$, PO_4 and NO_3 was measured daily in triplicate to monitor the performance of the analyser. Also measured was Reference Material for Nutrients in Seawater (RMNS; batch AZ from KANSO; www.kanso.co.jp/eng/production) for international consistency. The reported NO_3 may in some samples comprise a very small amount of NO_2 that is not distinguished and thus is incorporated into 'NO_3' when described in the text. The precision values (expressed as the coefficient of variation) for $Si(OH)_4$, PO_4 and NO_3 are estimated as 0.29%, 0.27% and 0.30%, respectively. The carbon and nutrient data are included in the GLODAPv2 data product

(Olsen *et al.* 2019), which, according to stringent GLODAPv2 quality control measures, did not need any adjustments and thus are of high quality.

Seasonal changes

Seasonal changes in C_T and A_T were estimated from depth profiles (Fig. 3), using the difference between the average summer mixed-layer concentrations and the inferred winter concentrations from the observed concentrations at the depth of the temperature minimum, the latter taken to represent the remnant of the Winter Water (e.g. Jones *et al.* 2011, Tynan *et al.* 2016). The total seasonal change in C_T (ΔC_T) and A_T (ΔA_T) results from the influences of the main physical and biological processes, such as salinity changes ($\Delta C_{T\ sal}$, $\Delta A_{T\ sal}$) from freshwater inputs and mixing of different water masses, photosynthesis and respiration ($\Delta C_{T\ org}$, $\Delta A_{T\ org}$) and the formation and dissolution of biotic (aragonite, calcite) and abiotic (ikaite) calcium carbonate ($\Delta C_{T\ CaCO3}$, ΔA_T*).

$$\Delta C_T = \Delta C_{T\ sal} + \Delta C_{T\ org} + \Delta C_{T\ CaCO3} \quad (6)$$

$$\Delta A_T = \Delta A_{T\ sal} + \Delta A_{T\ org} + \Delta A_T^* \quad (7)$$

Salinity normalization of C_T and A_T ($C_{T\ sal}$ and $A_{T\ sal}$) was carried out using the normalization method that accounts for non-zero C_T and A_T freshwater endmembers and a reference salinity (34.68; S_{ref}) of uCDW (Friis *et al.* 2003). The freshwater endmember for sea ice (C_T = 277 ± 150 μmol kg^{-1}; A_T = 328 ± 150 μmol kg^{-1}) from Legge *et al.* (2017), obtained from land-fast sea ice adjacent to Adelaide Island, was used. The values of $\Delta C_{T\ sal}$ and $\Delta A_{T\ sal}$ are determined from the difference between the total and salinity-normalized changes. It is assumed here that $\Delta C_{T\ sal}$ and $\Delta A_{T\ sal}$ integrate the signal from salinity changes due to freshwater inputs (e.g. meltwater) and advection, mixing and upwelling of different water masses.

Changes in C_T due to photosynthetic fixation of C_T and production of organic matter ($\Delta C_{T\ org}$) were determined from changes in salinity-normalized NO_3 and the classical C/N Redfield ratio of 106/16 = 6.6 (Redfield 1958), which appears to be valid for the Southern Ocean (Hoppema & Goeyens 1999). Following Redfield stoichiometry (Redfield 1958), a decrease in C_T of 1 μmol kg^{-1} due to phytoplankton uptake is accompanied by a decrease of 16/106 = ~0.15 μmol kg^{-1} nitrate, which causes a ~0.15 μmol kg^{-1} increase in A_T (Dickson 1981, Sarmiento & Gruber 2006). The $\Delta A_{T\ org}$ is therefore estimated from $\Delta C_{T\ org}$ by applying 0.15 μmol A_T kg^{-1} per 1 μmol C_T kg^{-1} removed during photosynthetic production of organic matter. It has been argued that the uptake of the macronutrients of phosphorus (P) and sulphur (S) would also affect A_T (Wolf-Gladrow *et al.* 2007). This would lead to a higher uptake ratio of 21.8/106 and an ensuing increase in A_T of ~0.21 μmol kg^{-1} ($\Delta A_{T\ org}$) per 1 μmol kg^{-1} $\Delta C_{T\ org}$. The average difference between $\Delta A_{T\ org}$ determined from $\Delta C_{T\ org}$ using both ratios was 2.7 ± 1.7 μmol kg^{-1}. This would lead to average increases in $\Delta\Omega_{aragonite\ org}$ of ~0.02, which is ~4% of the total $\Delta\Omega_{aragonite\ org}$ value and yields negligible difference from the result of this study. This is due to $\Delta\Omega_{aragonite\ org}$ being dominated by $\Delta C_{T\ org}$, so fractional adjustments in $A_{T\ org}$ have a very small effect on $\Delta\Omega_{aragonite\ org}$. Thereby, we adhere to the uptake ratio of 16 and the ensuing change of 0.15 μmol A_T kg^{-1} per 1 μmol C_T kg^{-1} removed during photosynthesis.

The $\Delta C_{T\ CaCO3}$ accounts for any calcium carbonate mineral (biotic aragonite and calcite; abiotic ikaite) formation or dissolution that changes the A_T:C_T ratio by 2:1 (Dickson 1981, Broecker & Peng 1982, Sarmiento & Gruber 2006). This is determined from potential alkalinity (A_T*), which is the sum of salinity-normalized A_T and NO_3 (Goldman & Brewer 1980 and references cited therein) following Jones *et al.* (2017). The A_T* accounts for salinity changes and the increase (decrease) in A_T of 1 μmol kg^{-1} due to the uptake (release) of 1 μmol kg^{-1} NO_3 during photosynthesis (respiration), as described above (Broecker & Peng 1982,

Sarmiento & Gruber 2006). Thus, $\Delta C_{T\ CaCO3} = 0.5\ \Delta A_T^*$. It is acknowledged that from the dissolved constituents in seawater, and further calculated seawater tracers, the changes of such variables can be ascribed to the formation/dissolution of carbonate minerals but cannot define specifically which one, two or all three of the relevant minerals (aragonite, calcite or ikaite) is the carbonate source involved without the isolation and identification of such minerals. Hence, the role of other polymorphs, such as high-Mg calcite, and the identification of the carbonate source (e.g. aragonite, calcite or ikaite) with varying elemental ratios in solid $CaCO_3$ is beyond the scope of this work.

The seasonal changes in C_T and A_T (ΔC_T and ΔA_T) for each of the key processes were used to determine perturbations in summer mixed-layer Ω ($\Delta\Omega_{aragonite}$ and its partial constituents $\Delta\Omega_{aragonite\ sal}$, $\Delta\Omega_{aragonite\ org}$ and $\Delta\Omega_{aragonite\ CaCO3}$) alongside *in situ* temperature, salinity and macronutrient concentrations with the *CO2SYS* program. The different process-driven $\Delta\Omega$ values are used alongside the A_T:C_T ratio as indicators of the buffering capacity of seawater to estimate the impacts of the changes on the aragonite saturation state.

Uncertainties in analytical and calculation techniques

Uncertainties associated with the analytical measurements of the total ΔC_T (Eq. (6)) and ΔA_T (Eq. (7)) were based on analytical precision (C_T ± 1.0 μmol kg^{-1}; A_T ± 1.5 μmol kg^{-1}) and estimated as ± 2 and ± 3 μmol kg^{-1}, respectively. Uncertainties in $\Delta C_{T\ sal}$ and $\Delta A_{T\ sal}$ were estimated, by consideration of the uncertainty in the endmember (± 150 μmol kg^{-1}; Legge *et al.* 2017) and by maximum difference between measured and salinity-normalized values (± 6 μmol kg^{-1}), as ± 8 and ± 9 μmol kg^{-1}, respectively. Uncertainties in $\Delta C_{T\ org}$ and $\Delta A_{T\ org}$ were estimated from the analytical precision of NO_3, where an upper bound of the error for $\Delta NO_{3\ sal}$ was set to ± 0.11 μmol kg^{-1}; thus, the equivalent for $C_{T\ org}$ was ± 0.7 μmol kg^{-1} and for $A_{T\ org}$ was ± 0.1 μmol kg^{-1}. By applying an uncertainty in the C/N ratio, which was set to ± 1 μmol kg^{-1} to account for deviations in the ratio compared with Redfield stoichiometry (e.g. Hoppema & Goeyens 1999), the compound upper-bound uncertainty for $\Delta C_{T\ org}$ and $\Delta A_{T\ org}$ was ± 1.7 μmol kg^{-1} and for $A_{T\ org}$ was ± 1.1 μmol kg^{-1}. Upper-bound uncertainties in ΔA_T^* and $\Delta C_{T\ CaCO3}$ were estimated from the combined uncertainty of salinity-normalized A_T (± 6 μmol kg^{-1}) and NO_3 (± 0.09 μmol kg^{-1}) as ± 12 μmol kg^{-1}. Using the same approach, uncertainties associated with the $\Delta\Omega_{aragonite}$ partial contributions were estimated from the associated errors for each ΔC_T and ΔA_T term in *CO2SYS*: $\Delta\Omega_{aragonite\ sal}$ ± 0.29, $\Delta\Omega_{aragonite\ org}$ ± 0.05 and $\Delta\Omega_{aragonite\ CaCO3}$ ± 0.41. Uncertainties in $\Omega_{aragonite}$ determined from the use of different equilibrium constants (K_1 and K_2; e.g. Mojica Prieto & Millero 2002, relative to those of Mehrbach *et al.* 1973 refit by Dickson & Millero 1987) were estimated in *CO2SYS* as ± 0.04, which is of similar magnitude to the range of uncertainties determined above.

Results

Sea surface waters

The summer surface waters in the region were relatively warm and fresh (Fig. 3a & b), with salinities ranging from 33.41 to 33.95 and potential temperatures of 0.56–2.03°C. Warmer and more saline waters were observed on the shelf compared to offshore, with the exception of the freshest surface water that occurred closest to the coast near Anvers Island and Adelaide Island (Fig. 1a). The surface waters exhibited distinct changes in biogeochemical properties from north to south and between offshore and the shelf region (Fig. 1b–g). Values of C_T varied between 2080 and 2158 μmol kg^{-1}, with lower concentrations in the south (Fig. 3c). Closest to the coast, lower C_T was coincident with low-salinity waters. Congruent with the distribution of salinity, A_T increased from 2273 μmol kg^{-1} offshore to the highest values of 2305 μmol kg^{-1} over the shelf (Fig. 3d). An exception

was lower A_T (2287 μmol kg^{-1}) near Anvers Island. Salinity-normalized C_T ($C_{T\ sal}$) varied by ~60 μmol kg^{-1} and was lowest (2142 μmol kg^{-1}) on the southernmost transect as an indicator of the larger influence of biological carbon uptake in the south relative to the north (Fig. 1b). In contrast, salinity-normalized A_T ($A_{T\ sal}$) varied by ~30–40 μmol kg^{-1} from the lowest values offshore to higher values of 2375 μmol kg^{-1} over the shelf where the impact of freshwater inputs was greatest in coastal waters (Fig. 1c). Low $NO_{3\ sal}$ (< 10 μmol kg^{-1}) occurred in the south and close to the coast as a result of biological drawdown (Fig. 1d), coinciding with low C_T. Closely following patterns in A_T, values of $Si(OH)_{4\ sal}$ increased by > 30 μmol kg^{-1} from offshore surface waters to the highest value of 59.4 μmol kg^{-1} over the shelf (Fig. 1e). The highest carbonate mineral saturation states were found over the shelf, with the highest values for $\Omega_{calcite}$ (3.68) and $\Omega_{aragonite}$ (2.31) closest to the coast (Fig. 1f & g). The degree of saturation in surface waters increased southwards from the lowest levels of $\Omega_{calcite}$ (2.39) and $\Omega_{aragonite}$ (1.50) offshore. The A_T:C_T ratio (Fig. 3h) ranged from 1.06, implying a reduced buffering capacity where A_T was lowest offshore, to 1.11 and an increased buffering capacity with higher A_T and lower C_T in the shelf region.

Water masses of the West Antarctic Peninsula

The vertical distribution of potential temperature and salinity identified the fresher AASW, cold Winter Water (with winter temperatures closer to freezing point) and warm core of uCDW in the ACC overlying cold, saline deep waters (Fig. 2 & Table I). Projections of uCDW that extended over the shelf mixed with Winter Water and formed the cooler and fresher variety of uCDW, modified CDW (mCDW) . Water column A_T, C_T and macronutrients showed reductions in the AASW and seasonal mixed layer as compared to the underlying Winter Water for both the shelf and offshore regions. The vertical distribution of A_T aligned well with that of salinity (Fig. 2b, h & n). The region was dominated by the C_T-rich CDW, with the lowest A_T:C_T ratios in the uCDW offshore (Fig. 2c, i & o). Macronutrients increased with depth and showed that the shelf region had generally lower NO_3 and higher $Si(OH)_4$ compared with offshore waters (Fig. 2d, j & p). The distribution of $\Omega_{calcite}$ (Fig. 2e, k & q) and $\Omega_{aragonite}$ (Fig. 2f, l & r) reflected the differences in C_T and A_T, with higher values (saturation) in the upper layers, especially over the shelf, and the lowest values (undersaturation) in deep waters.

Seasonal mixed layer

The AASW reflected seasonal warming (average θ = 0.30–1.04°C) and freshwater inputs (average S = 33.77–33.92) in the upper part of the water column compared to the Winter Water beneath (Fig. 3a & b & Table I). Summer MLDs (above the seasonal pycnocline) ranged between 7 and 107 m, being shallower and fresher over the shelf compared to offshore. The distribution of C_T (Fig. 3c) and NO_3 revealed spatial variability with lower values over the shelf and averages of 2136 ± 11 and 19.1 ± 5.2 μmol kg^{-1}, respectively, in the south transect (ST). In contrast, values of A_T (Fig. 3d) and $Si(OH)_4$ exhibited notable cross-shelf variability and were higher at 2305 ± 3 and at 54.3 ± 4.6 μmol kg^{-1}, respectively, over the shelf relative to offshore waters. Values of $C_{T\ sal}$ were distinctly lower over the southern shelf region (ST) and $A_{T\ sal}$ was elevated over the shelf, particularly in the north transect (NT). The AASW was most saturated with carbonate minerals with $\Omega_{calcite}$ of 2.78 ± 0.48 and $\Omega_{aragonite}$ of 1.74 ± 0.30 (Fig. 3g) over the shelf in the south. This was accompanied by the highest A_T:C_T ratio (Fig. 3h). Conversely, the lowest $\Omega_{calcite}$, $\Omega_{aragonite}$ and low A_T:C_T ratio values occurred in offshore AASW in the north.

Deeper convective mixing during the previous winter was evident over the shelf as Winter Water depths increased up to 136 m depth compared with offshore waters. This was accompanied by warmer and saltier (-0.65 ± 0.64°C, 34.05 ± 0.08) Winter Water over the shelf (Fig. 3a & b) compared with offshore waters (-1.07 ± 0.42°C, 33.95 ± 0.07). Winter Water values of C_T and A_T over the shelf were 2195 ± 16 and 2311 ± 5 μmol kg^{-1}, respectively, and there were higher than average offshore Winter Water

values of C_T and A_T of 2184 ± 10 and 2295 ± 8 μmol kg^{-1}, respectively (Fig. 3c & d). Winter Water $C_{T\,sal}$ and $A_{T\,sal}$ were slightly lower and higher, respectively, compared to C_T and A_T (Fig. 3e & f). Concentrations of NO_3 were lower over the shelf (27.0 ± 1.9 μmol kg^{-1}) compared to offshore (29.0 ± 1.1 μmol kg^{-1}), and $Si(OH)_4$ was clearly higher over the shelf (68.9 ± 4.8 μmol kg^{-1}) compared to offshore (44.1 ± 7.8 μmol kg^{-1}). A latitudinal gradient showed that the Winter Water potential temperature decreased by ~1°C from the north (NT) to south (ST). Values of $\Omega_{aragonite}$ varied between 1.15 and 1.46 (Fig. 3g), with the lowest values close to the coast near Adelaide Island. Values of $\Omega_{calcite}$ varied between 1.83 and 2.33 in the upper mixed layer (not shown). The A_T:C_T ratio ranged from 1.04 to 1.06 (Fig. 3h).

Circumpolar Deep Water

The subsurface potential temperature maximum ($1.70 \leq \theta \leq 2.13$°C; $34.54 \leq S \leq 34.75$) identified the offshore core of uCDW (Table I) in the ACC, which extended to the shelf break (Fig. 2). Concurrent potential temperature maxima over the shelf were cooler and fresher compared to the ACC-derived uCDW, which distinguished the mCDW (typically $34.6 \leq S \leq 34.7$). Comparable increasing gradients in C_T and A_T were seen between the Winter Water and subsurface uCDW and mCDW (Fig. 3c & d). The variability in $Si(OH)_4$ in the water column was similar to that of A_T, as shelf waters had higher concentrations, especially in the 400–600 m depth range compared with offshore waters. The average NO_3 in both offshore and shelf regions was similar at ~33 μmol kg^{-1}. The mCDW was characterized by signatures of remineralization and upwelled deeper waters across the shelf break with higher C_T (2264 ± 7 μmol kg^{-1}), A_T (2350 ± 5 μmol kg^{-1}) and $Si(OH)_4$ (102.8 ± 7.8 μmol kg^{-1}) compared with uCDW values of C_T (2253 ± 3 μmol kg^{-1}), A_T (2347 ± 5 μmol kg^{-1}) and $Si(OH)_4$ (85.0 ± 3.7 μmol kg^{-1}). Within the uCDW and mCDW cores, the A_T:C_T ratio was lowest with values of 1.03–1.05. Subsurface concentrations of $C_{T\,sal}$ and $A_{T\,sal}$ on the shelf were ~5–30 μmol kg^{-1} higher compared with those offshore (~2253 μmol C_T kg^{-1}, ~2347 μmol A_T kg^{-1}). The highest $C_{T\,sal}$ (2276 μmol kg^{-1}) was found at 400 m depth in the south (ST).

Carbonate mineral saturation showed a general latitudinal decrease from north to south with $\Omega_{calcite}$ always above saturation. The $\Omega_{aragonite}$ was close to saturation levels in uCDW (1.06 ± 0.04) and mCDW (1.07 ± 0.05). The aragonite saturation horizon ($\Omega_{aragonite} = 1.0$) shoaled over the shelf where $\Omega_{aragonite}$ was showing slight undersaturation at 0.97 at 430 m depth in the southern region.

Deep waters offshore

Deep waters (depths > 2000 m) in the ACC in the offshore region (Fig. 2), which included lower CDW, were characterized by C_T (2261 ± 2 μmol kg^{-1}), A_T (2367 ± 2 μmol kg^{-1}) , NO_3 (32.3 ± 0.2 μmol kg^{-1}) and $Si(OH)_4$ (131.8 ± 6.5 μmol kg^{-1}). Deep waters were all undersaturated with respect to aragonite ($\Omega_{aragonite}$ of 0.54–0.86), and the saturation horizon for calcite ($\Omega_{calcite} = 1$) was found at ~3000 m depth. The A_T:C_T ratio ranged between 1.04 and 1.05, showing a slightly higher buffering capacity compared with the overlying uCDW. The latitudinal distribution of deep water revealed variability as the isotherms were more steeply inclined towards the continental slope in the NT region, which is less apparent in the central transect (CT) region and almost absent in the ST region. This resulted in a southwards increase in the average potential temperature of waters in the 2000–2500 m depth range from 0.68°C ± 0.25°C to 0.74°C ± 0.12°C. This was accompanied by a slight increase in salinity and reduction in C_T and $Si(OH)_4$.

Inorganic carbon and nutrient cycling

The relationships between A_T, C_T and macronutrients (Fig. 4) revealed different biogeochemical regimes in the different water masses and offshore and shelf regions. The highest A_T, high C_T and the lowest $\Omega_{aragonite}$ at ~0.5 distinguished the deep and bottom waters offshore (Fig. 4a). The highest C_T and near-undersaturation of aragonite ($\Omega_{aragonite} \approx 1$) defined the shelf region. Aragonite supersaturation ($\Omega_{aragonite} > 1.8$) was associated with the combination of the lowest C_T and elevated A_T over the shelf. The relationships between C_T and NO_3 (Fig. 4b) and between C_T and $Si(OH)_4$ (Fig. 4c) showed general trends with lowest concentrations co-occurring over the shelf and offshore, respectively, where $\Omega_{aragonite}$ was in the 1.6–2.3 range. Regional differences were clearly identified; the highest $Si(OH)_4$ and the highest NO_3 occurred in undersaturated ($\Omega_{aragonite} < 1$) deep and bottom waters offshore. The values of NO_3 and PO_4 (Fig. 4d) were closely coupled with the lowest values over the shelf associated with the highest $\Omega_{aragonite}$ of ~2.3. The lowest $Si(OH)_4$ (Fig. 4e) and reduced NO_3 concentrations occurred offshore with $\Omega_{aragonite}$ at ~1.8.

Relationships between inorganic carbon and nutrients in the seasonal mixed layer (AASW and Winter Water) for offshore waters were statistically significant and yielded ratio values (estimated from slopes of the linear regression) for C/N of 11.8 ± 0.7 (r^2 = 0.80, $P << 0.0001$, n = 72), C/Si of 1.0 ± 0.1 (r^2 = 0.76, $P << 0.0001$, n = 72), N/P of 12.9 ± 0.2 (r^2 = 0.98, $P << 0.0001$, n = 72) and Si/N of 7.3 ± 1.1 (r^2 = 0.39, $P < 0.001$, n = 72). For the shelf region, nutrient uptake ratios were also estimated from statistically significant relationships with C/N of 10.6 ± 0.6 (r^2 = 0.89, $P << 0.0001$, n = 48), C/Si of 1.2 ± 0.1 (r^2 = 0.68, $P <$ 0.0001, n = 48), N/P of 13.8 ± 0.3 (r^2 = 0.98, $P << 0.0001$, n = 48) and Si/N of 4.8 ± 0.9 (r^2 = 0.40, $P < 0.001$, n = 48). The carbon and nutrient ratio values in the shelf region were lower for C/N and Si/N and higher for C/Si and N/P compared with the offshore waters.

Seasonal mixed-layer physical and biological processes

Reductions in C_T, A_T and macronutrients in surface water and the seasonal mixed layer compared to the Winter Water showed the impact of freshwater inputs in the shelf and offshore regions along the WAP (Fig. 2). Theoretical dilution lines between endmembers for uCDW, determined as average C_T and A_T in offshore CDW (S = 34.7, C_T = 2253 ± 3 μmol kg^{-1}, A_T = 2347 ± 3 μmol kg^{-1}) and for sea ice (C_T = 277 ± 150 μmol kg^{-1}, A_T = 328 ± 150 μmolkg^{-1}) and glacial ice (C_T = 16 ± 5 μmol kg^{-1}, A_T = 100 ± 5 μmol kg^{-1}) showed the influence of salinity changes on C_T and A_T in the full water column (Fig. 5a). The relationships between C_T and A_T with salinity in the seasonal mixed layer (AASW and Winter Water) yielded $C_T = 168S - 3530$ (r^2 = 0.90, SE = 176 μmol kg^{-1}, $P << 0.0001$, n = 120) and $A_T = 58S + 333$ (r^2 = 0.71, SE = 116 μmol kg^{-1}, $P << 0.0001$, n = 120). The distribution of A_T closely followed the dilution lines, with deviations showing increased A_T in some of the fresher, upper-ocean waters and increased A_T in salty, deeper waters. Elevated A_T in the freshest waters over the shelf indicated an additional A_T source to surface waters with respect to sea ice- and glacial ice-derived A_T. Values of C_T showed greater variability relative to the dilution lines with strong deviations showing reduced C_T due to biological carbon uptake in fresher, upper-ocean waters and increased C_T largely from respiration in saltier, deeper waters. This is further explored by consideration of $C_{T\,sal}$ and potential alkalinity (A_T*), where the seasonal mixed layer is strongly influenced by C_T uptake due to organic matter production with an imprint of $CaCO_3$ formation/dissolution (Fig. 5b). Deep waters are distinguished by elevated A_T and C_T as a result of $CaCO_3$ dissolution and respiration/remineralization, respectively.

The seasonal deficits in C_T and A_T (AASW *vs* Winter Water) for offshore and shelf waters were partitioned into the key driving physical and biological processes (Fig. 6). Shelf waters had greater and variable C_T deficits with an average ΔC_T of -69 ± 35 μmol kg^{-1} in comparison to offshore waters with an average ΔC_T of -44 ± 9 μmol kg^{-1} (Fig. 6a). The largest ΔC_T of -138 μmol

357 kg^{-1} occurred closest to the coast (Adelaide Island) in the south, which was dominated by $\Delta C_{T\ org}$ of -132 μmol kg^{-1} (Fig. 6c).
358 Values of ΔA_T varied between -1 and -23 μmol kg^{-1} (average ~ -10 μmol kg^{-1}) across the region (Fig. 6e). Freshwater inputs were
359 greatest in the shelf region with average $\Delta C_{T\ sal}$ and $\Delta A_{T\ sal}$ values of -12 ± 9 and -16 ± 11 μmol kg^{-1}, respectively (Fig. 6b & f).
360 The most notable freshwater impacts were closest to the coast in the north (Anvers Island), driving a maximum $\Delta C_{T\ sal}$ of -34
361 μmol kg^{-1} and $\Delta A_{T\ sal}$ of -37 μmol kg^{-1}. This was accompanied by the highest ΔA_T* of 6 μmol kg^{-1} and an associated $\Delta C_{T\ CaCO3}$
362 of 3 μmol kg^{-1} (Fig. 6d & h). The average $\Delta C_{T\ org}$ over the shelf was -58 ± 42 μmol kg^{-1}, which was generally larger and more
363 variable compared with the average $\Delta C_{T\ org}$ of -37 ± 9 μmol kg^{-1} offshore. The $\Delta A_{T\ org}$ followed similar spatial trends with a
364 maximum $\Delta A_{T\ org}$ of 19 μmol kg^{-1} coinciding with largest C_T deficits over the shelf (Fig. 6g). The ΔA_T* and $\Delta C_{T\ CaCO3}$ were ≤ 0
365 μmol kg^{-1} in offshore waters and were lowest at -12 and -6 μmol kg^{-1}, respectively, in the north.

366 Changes in $\Omega_{aragonite}$ between Winter Water and the summer mixed layer ($\Delta\Omega_{aragonite}$) reflected the combined effects of ΔC_T and
367 ΔA_T in the offshore and shelf regions and distinct latitudinal variability (Fig. 7). The $\Delta\Omega_{aragonite}$ ranged between 0.20 in offshore
368 waters in the north and as much as 1.15 over the shelf in the south (Fig. 7a). Salinity changes had minor effects on $\Delta\Omega_{aragonite}$
369 across the region as $\Delta\Omega_{aragonite\ sal}$ was 0.02 ± 0.01 (Fig. 7b), indicating that dilution effects on A_T (reduced $\Omega_{aragonite}$) were
370 counteracted by concomitant reductions in C_T (increased $\Omega_{aragonite}$). A higher average $\Delta\Omega_{aragonite}$ (0.54 ± 0.31) in shelf waters was
371 driven by biological carbon uptake, with the highest $\Delta\Omega_{aragonite\ org}$ of 1.39 near Adelaide Island (Fig. 7c). Offshore waters had a
372 lower average $\Delta\Omega_{aragonite}$ (0.31 ± 0.08) as a result of decreases in mixed-layer carbonate (negative ΔA_T*) as $\Delta\Omega_{aragonite\ CaCO3}$
373 (changes in $\Omega_{aragonite}$ due to the processes of any $CaCO_3$ mineral) was -0.02 in the north (Fig. 7d). The lowest $\Delta\Omega_{aragonite\ sal}$ (~0)
374 occurred with the greatest freshening signal in shelf waters near Anvers Island and was accompanied by the highest $\Delta\Omega_{aragonite}$
375 $_{CaCO3}$ (0.07). Residual changes in $\Delta\Omega_{aragonite}$, determined from the difference in the total seasonal change and other contributing
376 factors, were on average -0.12 ± 0.09 and represented a reduction in AASW $\Omega_{aragonite}$ relative to Winter Water $\Omega_{aragonite}$. Changes
377 in $\Omega_{calcite}$ ($\Delta\Omega_{calcite}$; not shown) exhibited the same spatial variations as $\Delta\Omega_{aragonite}$ with a range of 0.32–1.83 and an average $\Delta\Omega_{calcite}$
378 in the shelf (offshore) region of 0.86 ± 0.50 (0.50 ± 0.13).

379 **Discussion**

380 *Meltwater influence on carbonate mineral saturation*

381 The seasonal changes in carbonate mineral saturation in the upper ocean reflected the spatial variability in C_T and A_T that created
382 distinct gradients in $\Omega_{aragonite}$ across the shelf from offshore and latitudinally along the WAP. The highest $\Omega_{aragonite}$ in fresher
383 surface waters close to the coast (Fig. 1) was accompanied by large salinity-driven seasonal deficits in A_T and C_T as a result of
384 freshwater dilution of A_T and C_T over the shelf. The WAP shelf is influenced by numerous marine-terminating glaciers and is
385 located in the seasonal sea-ice zone whereby glacial meltwater, snow and melting sea ice seasonally supply the continental shelf
386 with freshwater (Meredith *et al.* 2013). The impacts of freshwater on A_T and C_T are revealed from the close relationships of both
387 with salinity (Fig. 5). The variability of A_T was largely controlled by changes in salinity as driven by meltwater inputs (freshwater
388 endmember) and mixing with uCDW (saline endmember). Deviations from theoretical mixing lines were most pronounced
389 towards the two endmembers, where processes of photosynthesis/respiration and $CaCO_3$ precipitation/dissolution were shown
390 to play important roles in controlling A_T. The shelf region experienced a greater influence of freshwater as indicated by salinity-
391 driven reductions in C_T and particularly A_T ($\Delta C_{T\ sal\ shelf}$ = -12 ± 9 μmol kg^{-1}; $\Delta A_{T\ sal\ shelf}$ = -16 ± 11 μmol kg^{-1}; Fig. 6) that exceeded
392 those in offshore waters ($\Delta C_{T\ sal\ offshore}$ and $\Delta A_{T\ sal\ offshore} \approx$ -10 μmol kg^{-1}). Mixing of seawater with sea-ice or glacial meltwater

leads to a dilution of carbonate ions, with the potential to drive a decrease in $\Omega_{aragonite}$ due to the lower A_T and C_T signatures in the fresh meltwater compared with seawater (Legge *et al.* 2017). However, surface waters were oversaturated with respect to aragonite, whereby reductions in surface-layer salinity actually contributed to an increased mixed-layer $\Omega_{aragonite}$ of 0.02 ± 0.01 (Fig. 7). These salinity-driven changes revealed the effects of combined A_T and C_T variability on $\Omega_{aragonite}$ as the dilution and reduction of A_T (reducing $\Omega_{aragonite}$) were counteracted by the parallel dilution and reduction of C_T (increasing $\Omega_{aragonite}$). The seasonal meltwater release contributed to net increases in $\Omega_{aragonite}$ to create spatial gradients in surface water calcium carbonate saturation during summer, which supports previous findings along the WAP (Hauri *et al.* 2015, Jones *et al.* 2017, Legge *et al.* 2017) and in the Southern Ocean region to the north-east of the WAP (e.g. Jones *et al.* 2011, Tynan *et al.* 2016).

Biological production drives carbonate mineral supersaturation

Reductions in salinity-normalized C_T and NO_3 occurred along the meltwater-influenced shelf, particularly in the vicinity of Anvers Island and Adelaide Island (Fig. 1), indicating the stronger influence of biological carbon uptake and the production of organic matter in the nearshore region. Biological carbon uptake of up to 132 μmol kg^{-1} dominated the seasonal changes in $\Omega_{aragonite}$ (at least 93% of $\Delta\Omega_{aragonite}$; Fig. 7) to counteract any meltwater-induced suppression of carbonate mineral saturation states ($\Delta\Omega_{aragonite\ bio} > \Delta\Omega_{aragonite\ sal}$). Large phytoplankton blooms are known to occur along the WAP shelf during spring and summer (Vernet *et al.* 2008, Schofield *et al.* 2017), where enhanced productivity characterizes the coastal regions such as near Anvers Island and Adelaide Island (Clarke *et al.* 2008, Trimborn *et al.* 2015). The highest chlorophyll *a* concentrations of up to 30 μg l^{-1} and elevated rates of primary production of 98–183 mg C m^{-3} day^{-1} were found in diatom-dominated blooms that occurred in summer 2011 in the south near Adelaide Island (Trimborn *et al.* 2015). The enhanced nearshore phytoplankton production resulted in biologically driven decreases in C_T with $\Delta C_{T\ org}$ of -58 ± 42 μmol kg^{-1} and associated increases in $\Delta A_{T\ org}$ (Fig. 6) and increased $\Omega_{aragonite}$ by 1.39 (Fig. 7) despite the influence of freshwater along the shelf. These processes created substantial summertime sinks for atmospheric CO_2 of > 40 mmol m^{-2} day^{-1} (Tortell *et al.* 2015). The shelf and coastal phytoplankton communities typically consist mainly of large diatoms, which was the case in summer 2011 as diatoms were dominant (> 70%) and accounted for most of the phytoplankton biomass and primary production (Trimborn *et al.* 2015). Enhanced productivity in this region is associated with glacial, sea-ice and snowmelt plumes that increase water column stratification, create favourable light conditions and supply nutrients to the surface layer (Vernet *et al.* 2008). As such, the combined effect of meltwater release and biological carbon uptake during the seasonal sea-ice melt period generated gradients in $\Omega_{aragonite}$ in the AASW across the shelf from offshore (Fig. 1). These findings support previous observations of high $CaCO_3$ saturation states in productive shelf and coastal waters during summer along the WAP (Hauri *et al.* 2015, Jones *et al.* 2017, Legge *et al.* 2017) and downstream of islands in the Southern Ocean (Tynan *et al.* 2016).

The distribution of $\Delta\Omega_{aragonite\ org}$ for the shelf region (average $\Delta\Omega_{aragonite\ org}$ on the shelf was 0.62 ± 0.44) showed latitudinal variability ranging from 0.42 ± 0.22 in the north to 1.00 ± 0.54 in the south (Fig. 7). This reflects a temporal signal of summertime phytoplankton production with an earlier onset of blooms in the north, following increasing light levels at the lower latitude, compared to the south. This probably accounts for the wide range of NO_3 concentrations that occurred in AASW (8.1–26.8 μmol kg^{-1}; Fig. 3) in shelf waters, as the lowest concentrations in the south capture the more recent signal of biological drawdown *vs* the influence of resupply from recycling and mixing with subsurface waters in the north (Henley *et al.* 2018). Nutrient concentrations were replete across the region between Anvers Island and Adelaide Island and showed that they were not limiting

to primary production, as reported previously (Henley *et al.* 2018). Our observations do not preclude limiting conditions later in the austral growing season as the latter has not finished by the end of January.

The statistically significant correlation between inorganic carbon and nutrients in the seasonal mixed layer indicated that drawdown during primary production was a key process controlling concentrations during summer (Fig. 4). The observed C/N ratios of 11.8 ± 0.7 and 10.6 ± 0.6 for offshore and shelf waters, respectively, were higher than the Redfield ratios, probably due to the effect of air-sea CO_2 uptake and subsequent influx of C_T in surface waters from strong summertime CO_2 sinks (Hauri *et al.* 2015, Tortell *et al.* 2015). The cycling of NO_3 and PO_4 was closely coupled with the lowest macronutrient concentrations over the shelf associated with a biologically driven high $\Omega_{aragonite}$ value of ~2.3 (Fig. 1). The observed N/P ratios of 12.9 ± 0.2 for offshore waters and 13.8 ± 0.3 for the shelf region indicate that the inorganic carbon and nutrient cycles depart from the Redfield stoichiometric value of 16 mol N (1 mol P)$^{-1}$ (Redfield 1958). The seasonal seawater N/P uptake ratios of ~13–14 probably result from the prevalence of diatoms along the WAP in summer 2011, which are known to exhibit lower N/P ratios compared with Redfield ratios and are consistent with previous findings (Clarke *et al.* 2008, Trimborn *et al.* 2015). The N/P uptake ratio values are within the range of those previously reported for the WAP region (N/P of 11.7–14.6; Hauri *et al.* 2015, Henley *et al.* 2018) and for the coastal waters of Adelaide Island (N/P of 11.1–15.3; Clarke *et al.* 2008).

Substantial decreases in concentrations of chlorophyll *a* to < 1 μg l^{-1} and lower rates of primary production of 3–9 mg C m^{-3} day^{-1} were observed in offshore waters (Trimborn *et al.* 2015). As for the shelf and coastal regions, diatoms were predominant in offshore waters (> 60%), whereas *Phaeocystis* accounted for ~20–40% of the biomass (Trimborn *et al.* 2015). The negative biological gradients across the WAP shelf are driven by concentrations of dissolved iron and reduced light levels from wind-driven deep mixing and the interaction between these two controlling factors (Dinniman *et al.* 2020 and references therein). The offshore phytoplankton communities during summer 2011 were exposed to lower dissolved iron concentrations compared with nearshore communities and exhibited physiological traits that indicate iron stress, perhaps coupled with light limitation in mixed layers up to 80 m deep (Trimborn *et al.* 2015). For this depth limit of offshore mixed layers, seawater N/P uptake ratios were reduced to 9.6 ± 0.4 (r^2 = 0.94, $P << 0.0001$, n = 48) and provided a further indication of impeded nitrate assimilation induced by iron limitation during blooms of large diatoms in the Southern Ocean.

The Si/N uptake ratios that were greater than 1Si:1N are indicative of large bloom-forming Antarctic diatoms that tend to be very heavily silicified (e.g. Tréguer *et al.* 2018). The Si/N uptake ratios were much higher than expected for diatom production alone, reflecting the presence of other phytoplankton species (e.g. *Phaeocystis*) and that additional processes (e.g. terrestrial and sediment/porewater fluxes) had occurred and increased $Si(OH)_4$ relative to NO_3. Lower dissolved $Si(OH)_4$ in the water column offshore is further evidence for strong biological drawdown in diatom blooms where assimilation processes exceeded $Si(OH)_4$ resupply processes, in contrast to conditions of elevated $Si(OH)_4$ in parallel to diatom-dominated production on the shelf (Fig. 3). The close coupling of C_T and $Si(OH)_4$ (Fig. 4) indicates the key role of diatoms that drive intense oceanic CO_2 uptake in offshore and coastal areas of the WAP.

Remineralization and lowering of carbonate mineral saturation in subsurface waters

Subsurface values of C_T, A_T, $Si(OH)_4$ and, to a lesser extent, NO_3 increased across the shelf from offshore waters, which was most pronounced in the south (Fig. 2 & Table I). These features coincided with the steepest vertical gradients between productive surface waters to the underlying mCDW over the southern shelf (Fig. 3). Enhanced concentrations of macronutrients and C_T in cross-shelf CDW has been previously reported for the southern WAP and attributed to organic matter remineralization and

biogenic silica dissolution in the productive and diatom-dominated waters of the shelf and coastal areas (Jones *et al.* 2017, Henley *et al.* 2018). Enriched C_T and low $\Omega_{aragonite}$ distinguished the mCDW of the shelf region, resulting in a shoaling of the aragonite saturation horizon across the shelf break and aragonite undersaturation in the mCDW in the south (Fig. 2r). Compared with offshore waters, Winter Water on the shelf was generally located at greater depths, was more saline and was characterized by higher A_T and $Si(OH)_4$ and generally higher C_T concentrations. The elevated A_T, $Si(OH)_4$ and C_T of the Winter Water were indicative of mixing with underlying mCDW, where greater exchange between water masses probably takes place over the shallower shelf relative to offshore. This indicates that the upward mixing of mCDW into the seasonal mixed layer could also provide a supply of A_T into the Winter Water layer. The concentrations of $Si(OH)_4$ also increased in the uCDW-mCDW layer across the shelf break (Fig. 2), indicating that upwelling and mixing of saline, A_T-rich deeper waters may contribute to this signal (higher A_T:C_T ratios). Therefore, the values of A_T in AASW and Winter Water may become decoupled from C_T concentrations (Fig. 4) through mixing of A_T-rich water into surface waters where biological C_T uptake occurs.

The relationship between salinity and A_T shows a mixing trend between A_T-rich subsurface waters and the fresher surface waters (Fig. 5), where the highest A_T at high salinities originates from the influence of $CaCO_3$ dissolution in the deep and offshore bottom waters. Increases in potential A_T for a smaller range of $C_{T\,sal}$ revealed the influence of $CaCO_3$ dissolution in enriching A_T in subsurface waters overlying the shelf (Fig. 5b). For C_T, the mixing trend shows increasing subsurface C_T concentrations over the shelf as a result of remineralization and a contribution from $CaCO_3$ mineral dissolution. The greater increase in subsurface C_T relative to increases in A_T with the cross-shelf modification of CDW drives lower A_T:C_T ratios and aragonite undersaturation in mCDW over the shelf (Fig. 2). Decoupling of Winter Water C_T and NO_3 with more saline waters over the shelf suggests that not solely remineralization but also sea-ice processes contribute, with brine rejection transporting C_T into the underlying water column during ice formation. Increasing A_T (for a small range of C_T) at salinities > 33.7 indicated carbonate mineral dissolution in Winter Water and evidence of a sea-ice carbon pump (Rysgaard *et al.* 2007, Dieckmann *et al.* 2008) over the shelf.

The coupling of inorganic carbon and nutrients at high concentrations (Fig. 4) in mCDW is driven by remineralization of organic matter and dissolution of biogenic silica exported from the productive surface layer (Henley *et al.* 2018 and references cited therein). Remineralization enriched C_T (reduced A_T:C_T ratios) and suppressed $\Omega_{aragonite}$ to yield a biologically induced acidification signal in subsurface water over the shelf (Fig. 2). Natural spatiotemporal variations in carbonate mineral saturation levels suggest that organisms of the WAP marine ecosystem are already exposed to low saturation states and as such may have evolved a degree of resilience to future acidification (Hauri *et al.* 2015, Legge *et al.* 2017). Enrichment of $Si(OH)_4$ in water masses overlying the shelf (Fig. 3j) was probably due to dissolution of biogenic silica from the diatom communities that characterized the summer blooms along the WAP (Trimborn *et al.* 2015). In addition, dissolved $Si(OH)_4$ from seafloor sediment resuspension and porewaters could contribute to elevated $Si(OH)_4$ concentrations in bottom waters (Henley *et al.* 2018). Mechanisms for elevated A_T in subsurface waters could also result from seafloor fluxes that provide a source of A_T to the deep and bottom waters overlying the shelf. In addition, upwelling of salty, A_T-rich deep waters onto the shelf would also increase the A_T:C_T ratios in upper shelf waters imprinted by the signal of biological C_T uptake.

Greater enhancements of the biogeochemical characteristics of mCDW in the southern shelf region relative to the north (Fig. 2) perhaps reflect 1) increases in C_T, NO_3 and $Si(OH)_4$ as a result of temporal variability in the more recent summer production, organic matter export and subsequent remineralization, 2) greater signals of salt and C_T in rejected brine from sea-ice formation during the preceding winter and 3) contributions of A_T and $Si(OH)_4$ from entrainment of deep waters, terrestrial minerals (e.g.

dissolved minerals delivered in glacial meltwater plumes), porewater and sediment sources. As such, the passage of uCDW from the offshore waters of the ACC across the shelf break enabled enrichment of regenerated C_T, thus lowering A_T:C_T ratios and $\Omega_{aragonite}$ in mCDW to drive a signal of biologically induced acidification over the WAP southern shelf.

Buffering against acidification on the freshwater-influenced shelf

Aragonite supersaturation ($\Omega_{aragonite} > 1.8$) occurred as a result of low $C_{T\ sal}$ and elevated $A_{T\ sal}$ in fresher surface waters over the shelf (Fig. 1). The A_T-salinity relationship (Fig. 5a) indicated that freshwater in the region contained a minor source of A_T, the value of which agreed very well with sea-ice A_T from fast ice at Rothera Research Station, Adelaide Island (Legge *et al.* 2017). Glacial ice was found to contain very low concentrations of macronutrients, C_T and A_T in the southern WAP region (Legge *et al.* 2017). The freshwater-derived A_T would be supplied to surface seawater from sea-ice and glacial melt along the coast and, coupled with biological uptake of C_T, would act to increase the A_T:C_T ratio. Meltwater plumes have been identified as sources of dissolved iron (e.g. Dinniman *et al.* 2020) to coastal waters due to dissolution and transport of minerals from the surrounding bedrock. This geochemical meltwater enrichment is considered a main source of iron to the WAP shelf region (Dinniman *et al.* 2020 and references cited therein) and may be subsequently important for the Antarctic coastal marine environment (Trimborn *et al.* 2015). Particulate and dissolved minerals incorporated into meltwater probably enrich the plumes with A_T relative to C_T, and they also become transport mechanisms of terrestrially derived organic matter that yields C_T upon remineralization. These land-meltwater-ocean processes lead to variations in the A_T:C_T ratio in the meltwater and upper ocean (Fig. 3h) upon mixing with the plume.

Sea ice near Adelaide Island contained varying concentrations of macronutrients, C_T and A_T (Legge *et al.* 2017) that are delivered to surface waters during the melt period, often with varying elemental stoichiometry compared with the source and surrounding seawater. Sea-ice processes play a key role in partitioning A_T and C_T differently within the ice and underlying water (Rysgaard *et al.* 2007, Dieckmann *et al.* 2008), and the variations in the A_T:C_T ratios exert geochemical control on $\Omega_{aragonite}$ in the winter and summer mixed layers in the seasonally ice-covered regions. During sea-ice formation, CO_2-rich brines are rejected, reducing the A_T:C_T ratio in the underlying Winter Water. Upon sea-ice melt, any ikaite minerals that were formed are released and, upon dissolution, provide a source of A_T in the meltwater and increase the A_T:C_T ratio in the surrounding surface seawater during spring and summer (Rysgaard *et al.* 2007, Dieckmann *et al.* 2008). Dissolution of ikaite during sea-ice melt has also been suggested as a mechanism contributing to A_T variability in summer surface waters in Southern Ocean regions north of the WAP (Jones *et al.* 2011, Tynan *et al.* 2016).

As for biogeochemical modifications to uCDW, strong cross-shelf gradients relative to offshore in terms of A_T in AASW and Winter Water were observed as a result of mixing of low-A_T meltwater and A_T-rich deep water (Fig. 2). The AASW with salinity of ~33.8 found offshore is characteristic of ACC water and is accompanied by an $A_{T\ sal}$ value of ~2345 μmol kg^{-1}, which was typically compared to shelf waters (Fig. 3). Cross-shelf increases in AASW salinity, indicative of upwelling and mixing with subsurface mCDW, was evident in the vicinity of the shelf break and coincided with a higher $A_{T\ sal}$ value of ~2355 μmol kg^{-1} (Fig. 2). Exceptions were an elevated $A_{T\ sal}$ value of ~2370 μmol kg^{-1} in meltwater-influenced surface waters that became superimposed onto the upwelling signal at coastal locations (Fig. 1). The values of $A_{T\ sal}$ increased by up to 40 μmol kg^{-1} in AASW overlying the shelf where the impact of meltwater was largest and dominated the seasonal change in A_T (ΔA_T; Fig. 6f) near Anvers Island and Adelaide Island. Variations in $A_{T\ sal}$ can be attributed to carbonate mineral processes in sea ice, terrestrially derived minerals in glacial meltwater plumes and runoff, benthic fluxes and a minor source during photosynthesis.

Evaluating potential alkalinity ($A_T^* = A_T + NO_3$; Goldman & Brewer 1980) allows the changes in A_T due to nitrate assimilation and inorganic nitrogen release to be accounted for, and remaining variations in A_T^* are due to carbonate mineral formation/dissolution (e.g. Jones *et al.* 2017). Elevated A_T^* (up to 10 μmol kg^{-1}; Fig. 5b) and increases in the A_T:C_T ratio in the coastal AASW (Fig. 3h) are consistent with a freshwater A_T source (e.g. terrestrially derived dissolved minerals in glacial meltwater, snowmelt and/or carbonate mineral dissolution in sea-ice meltwater).

Trends in A_T^* and salinity-normalized C_T (Fig. 5b) further indicated the role of carbonate mineral processes in controlling A_T in different water masses along the WAP. The shelf waters were biogeochemically distinct compared with offshore waters as a result of the greater contribution from calcium carbonate dissolution. This was reflected in the seasonal changes in calcium carbonate saturation states, with maximum increases in $\Omega_{aragonite}$ from $CaCO_3$ dissolution in the meltwater-influenced surface layers relative to Winter Water values (Fig. 7c). As the salinity normalization was carried out by considering the C_T and A_T signature of sea ice, the estimated increases in $A_{T\,sal}$ indicated that the contribution of A_T from the ice via the sea-ice carbon pump is probably variable within the ice and also varies with location (i.e. greater contributions over the southern shelf) and/or with contributions of A_T from terrestrial or benthic origin, as indicated previously by nutrient fluxes in the region (Henley *et al.* 2018). These processes make a small contribution to the seasonal changes in C_T (Fig. 6d). While surface water $C_{T\,sal}$ on the shelf was more depleted (higher A_T:C_T ratio) than in offshore waters (Fig. 1b), the $A_{T\,sal}$ in shelf waters (Fig. 1c) was elevated (higher A_T:C_T ratio). Both CO_2 drawdown during photosynthesis and the release of excess A_T increase the geochemical buffering capacity of seawater and drive calcium carbonate supersaturation ($\Omega_{aragonite} > 2.1$; $\Omega_{calcite} > 3.1$) in the relatively fresh surface waters on the shelf (Fig. 1). These processes that counteracted any meltwater suppression of saturation states and increased $\Omega_{aragonite}$ during the summer are consistent with other summer observations in coastal Antarctic waters (Jones *et al.* 2017, Legge *et al.* 2017).

Remote from freshwater influences, the lowest $\Omega_{aragonite}$ of ~1.5 occurred in AASW offshore north of 64°S (Fig. 1g). Concurrent high C_T (> 2140 μmol kg^{-1}), salinity (> 33.7) and temperature (> 1°C) indicated upwelling of uCDW in the region, with subsequent reduction of the A_T:C_T ratio and lowering of $\Omega_{aragonite}$ (Fig. 3). Weaker signals of biological C_T uptake relative to coastal and southern waters and the absence of 'excess' A_T in offshore surface waters would result in comparatively low surface water $\Omega_{aragonite}$. Seasonal differences in A_T^* revealed an overall loss of A_T of up to 10 μmol kg^{-1} (this being concomitant with decreases in C_T) in surface waters relative to the Winter Water. This indicates either the formation of carbonate minerals or another mechanism removing (adding) A_T from surface waters (Winter Water) by late summer. Playing a role here may be the aragonitic pteropods, which are prevalent along the WAP and are frequently observed at elevated abundances offshore in the study region (Thibodeau *et al.* 2019). Pteropods remove A_T in the upper water column through the formation of aragonite shells and release carbonate ions upon sinking and dissolution of the shells in deeper waters (Bednaršek *et al.* 2012). The 2:1 trend in A_T and C_T between Winter Water and AASW in the offshore region (Fig. 5b) could be due to the formation of calcium carbonate shells in the upper ocean and/or the supply of carbonates to the Winter Water from upwelling uCDW (with elevated carbonate from the dissolution of exported carbonate shells).

Conclusions and future outlook

This study gives insight into the spatial variability in calcium carbonate saturation states along the WAP, specifically the patterns in different water masses from offshore and across the continental shelf. Biological production in diatom-dominated blooms generated high $\Omega_{aragonite}$ and $\Omega_{calcite}$ with respect to the biotic minerals calcite and aragonite, respectively, along the WAP shelf in

summer. Glacial meltwater and melting sea ice stratified the water column and facilitated the formation of phytoplankton blooms, accompanied by elevated $\Omega_{aragonite}$ and $\Omega_{calcite}$ in surface waters close to the coast. The presence of excess A_T in the summer mixed layer indicates that dissolution of abiotic $CaCO_3$ (ikaite) from sea ice and/or terrestrially derived minerals in glacial meltwater has contributed to the surface water variability in $\Omega_{aragonite}$ and $\Omega_{calcite}$ during the seasonal thaw. The low A_T and C_T content of the meltwater dilutes the concentration of carbonate ions, thus tending to lower seawater $\Omega_{aragonite}$ and $\Omega_{calcite}$ and inducing a freshwater-driven acidification signal. However, additional dissolved constituents that contribute A_T relative to C_T slightly counteract the dilution effects by enhancing the A_T:C_T ratios in the meltwater-influenced seawater. Thus, any meltwater-driven carbonate ion dilution (tending to decrease A_T and the seawater buffering capacity) was largely compensated by biologically driven C_T uptake and excess A_T from dissolved minerals resulting in increases in $\Omega_{aragonite}$ and $\Omega_{calcite}$. These geochemical processes act as minor buffers against acidification and play a key role alongside the biological carbon uptake that drives increases in $\Omega_{aragonite}$ and $\Omega_{calcite}$ in coastal waters around Antarctica. Remineralization of organic matter and export of CO_2-rich brines from forming winter sea ice drive low $\Omega_{aragonite}$ and $\Omega_{calcite}$ in Winter Water and mCDW over the WAP shelf. A strong biological carbon pump in shelf waters and the coastal zone created surface water carbonate mineral supersaturation and biologically induced suppression of calcium carbonate saturation states in subsurface CDW. Mixing of water masses in the upper ocean suppresses surface water $\Omega_{aragonite}$ and may enhance the vulnerability of the surface layer to acidification upon further uptake of CO_2 and freshwater discharge. Given the increased and southwards shift in the upwelling of CDW, changes in sea-ice cover and oceanographic conditions in response to the El Niño Southern Oscillation and Southern Annular Mode, the WAP marine system will be even more vulnerable in the future.

Enhanced CO_2 drawdown in shelf waters may occur by 1) increased meltwater cooling of the surface layer that strengthens the solubility carbon pump, 2) releasing iron-rich terrigenous material in meltwater plumes to stimulate the biological carbon pump and 3) extended ice-free periods, enhanced water column stratification and favourable light environments that enhance the biological carbon pump. These processes have augmented the uptake of atmospheric CO_2 and supply of inorganic carbon to surface waters along the WAP in recent decades. However, the future outlook is uncertain as a result of the large variability and shifts in phytoplankton species and primary production, ice-ocean dynamics and freshwater fluxes and biogeochemical cycling, with consequences for the biologically driven and meltwater-driven changes in $\Omega_{aragonite}$ and $\Omega_{calcite}$ in the upper ocean. Our findings highlight the impact of high phytoplankton productivity, meltwater-derived mineral inputs and mixing of freshwater and CDW that regulate the spatial variability of calcium carbonate saturation states in the dynamic environment of the WAP. As such, the coastal zones of Antarctica are key regions for studying the response of marine ecosystems to impacts of ocean acidification. Spatiotemporal studies are therefore essential to elucidate the controls on calcium carbonate saturation states and to unravel the natural variability and long-term trends in order to better understand the impacts of future ocean acidification on marine ecosystems in the climatically vulnerable Antarctic coastal waters.

Acknowledgements

The authors gratefully acknowledge the Alfred Wegener Institute Helmholtz Centre for Polar and Marine Research for the opportunity to conduct fieldwork on board FS *Polarstern*. We acknowledge the leadership of the late E. Fahrbach (AWI) as chief scientist. Extended thanks to G. Rohardt at AWI and P. Laan, L. Salt and S. van Heuven at Royal NIOZ for scientific and logistical support. We thank Dr Matthew Humphreys and an anonymous reviewer for their thorough and insightful comments, which have greatly improved the quality of the manuscript.

Financial support

This work was part of postdoctoral research (E.M. Jones) at the Royal NIOZ supported through EU project CARBOCHANGE 'Changes in carbon uptake and emissions by oceans in a changing climate', which received funding from the European Community's Seventh Framework Programme under grant agreement no. 264879.

Author contributions

HJWdB and MH contributed to the conception and design of the study. EMJ, MH and KB contributed to the acquisition, analysis and interpretation of data. All authors drafted and/or revised the manuscript and approved the submitted version for publication.

Details of data deposit

All hydrographical data are publicly available in the Pangaea database (https://doi.org/10.1594/PANGAEA.772244).

References

ARRIGO, K.R., VAN DIJKEN, G. & LONG, M. 2008. Coastal Southern Ocean: a strong anthropogenic CO_2 sink. *Geophysical Research Letters*, **35**, 10.1029/2008gl035624.

BEDNARŠEK, N., TARLING, G., BAKKER, D., FIELDING, S., JONES, E.M., VENABLES, H.J., *et al.* 2012. Extensive dissolution of live pteropods in the Southern Ocean. *Nature Geoscience*, **5**, 10.1038/ngeo1635.

BROECKER, W.S. & PENG, T.H. 1982. *Tracers in the sea*. Palisades, NY: Eldigio Press.

BROWN, M.S., MUNRO, D.R., FEEHAN, C.J., SWEENEY, C., DUCKLOW, H.W. & SCHOFIELD, O.M. 2019. Enhanced oceanic CO_2 uptake along the rapidly changing West Antarctic Peninsula. *Nature Climate Change*, **9**, 10.1038/s41558-019-0552-3.

CLARKE, A., MEREDITH, M.P., WALLACE, M.I., BRANDON, M.A. & THOMAS, D.N. 2008. Seasonal and interannual variability in temperature, chlorophyll and macronutrients in northern Marguerite Bay, Antarctica. *Deep-Sea Research II*, **55**, 10.1016/j.dsr2.2008.04.035.

DICKSON, A.G. 1981. An exact definition of total alkalinity and a procedure for the estimation of alkalinity and total inorganic carbon from titration data. *Deep-Sea Research A*, **28**, 10.1016/0198-0149(81)90121-7.

DICKSON, A.G. & MILLERO, F.J. 1987. A comparison of the equilibrium constants for the dissociation of carbonic acid in seawater media. *Deep-Sea Research A*, **34**, 10.1016/0198-0149(87)90021-5.

DICKSON, A.G., SABINE, C. & CHRISTIAN, J.R. 2007. Guide to best practices for ocean CO_2 measurements. *PICES Special Publication*, No. 3, 1–191.

DIECKMANN, G.S., NEHRKE, G., PAPADIMITRIOU, S., GÖTTLICHER, J., STEININGER, R., KENNEDY, H., *et al.* 2008. Calcium carbonate as ikaite crystals in Antarctic sea ice. *Geophysical Research Letters*, **35**, 10.1029/2008GL033540.

DINNIMAN, M.S., ST-LAURENT, P., ARRIGO, K.R., HOFMANN, E.E. & VAN DIJKEN, G.L. 2020. Analysis of iron sources in Antarctic continental shelf waters. *Journal of Geophysical Research - Oceans*, **125**, e2019JC015736.

DUCKLOW, H.W., FRASER, W., MEREDITH, M., STAMMERJOHN, S., DONEY, S., MARTINSON, D., *et al.* 2013. West Antarctic Peninsula: an ice-dependent coastal marine ecosystem in transition. *Oceanography*, **26**, 10.5670/oceanog.2013.62.

FEELY, R.A., SABINE, C.L., LEE, K., BERELSON, W., KLEYPAS, J., FABRY, V.J. & MILLERO, F.J. 2004. Impact of Anthropogenic CO_2 on the $CaCO_3$ system in the oceans. *Science*, **305**, 10.1126/science.1097329.

FRIIS, K., KÖRTZINGER, A. & WALLACE, D.W.R. 2003. The salinity normalization of marine inorganic carbon chemistry data. *Geophysical Research Letters*, **30**, 10.1029/2002GL015898.

GOLDMAN, J. & BREWER, P.,1980. Effect of nitrogen source and growth rate on phytoplankton-mediated changes in alkalinity. *Limnology and Oceanography*, **25**, 10.4319/lo.1980.25.2.0352.

HALL, A. & VISBECK, M. 2002. Synchronous variability in the Southern Hemisphere atmosphere, sea ice, and ocean resulting from the Annular Mode. *Journal of Climate*, **15**, 10.1175/1520-0442(2002)015<3043:SVITSH>2.0.CO;2.

HAURI, C., DONEY, S.C., TAKAHASHI, T., ERICKSON, M., JIANG, G. & DUCKLOW, H.W. 2015. Two decades of inorganic carbon dynamics along the West Antarctic Peninsula. *Biogeosciences*, **12**, 10.5194/bg-12-6761-2015.

HENLEY, S.F., JONES, E.M., VENABLES, H.J., MEREDITH, M.P., FIRING, Y.L., DITTRICH, R., *et al.* 2018. Macronutrient and carbon supply, uptake and cycling across the Antarctic Peninsula shelf during summer. *Philosophical Transactions of the Royal Society*, **376**, 10.1098/rsta.2017.0168.

HOPPEMA, M. & GOEYENS, L. 1999. Redfield behaviour of carbon, nitrogen and phosphorus depletions in Antarctic surface water. *Limnology and Oceanography*, **44**, 10.4319/lo.1999.44.1.0220.

JONES, E.M., BAKKER, D.C.E., VENABLES, H.J., WHITEHOUSE, M.J., KORB, R.E. & WATSON, A.J. 2011. Rapid changes in surface water carbonate chemistry during Antarctic sea ice melt. *Tellus B*, **62**, 10.1111/j.1600-0889.2010.00496.x.

JONES, E.M., FENTON, M., MEREDITH, M.P., CLARGO, N.M., OSSEBAAR, S., DUCKLOW, H.W., *et al.* 2017. Ocean acidification and calcium carbonate saturation states in the coastal zone of the West Antarctic Peninsula. *Deep-Sea Research II*, **139**, 10.1016/j.dsr2.2017.01.007.

KERR, R., MATA, M.M., MENDES, C.R.B. & SECCHI, E.R. 2018. Northern Antarctic Peninsula: a marine climate hotspot of rapid changes on ecosystems and ocean dynamics. *Deep-Sea Research II*, **149**, 4–9.

LEGGE, O.J., BAKKER, D.C.E., MEREDITH, M.P., VENABLES, H.J., BROWN, P.J., JONES, E.M. & JOHNSON, M.T. 2017. The seasonal cycle of carbonate system processes in Ryder Bay, West Antarctic Peninsula. *Deep-Sea Research II*, **139**, 167–180.

MARTINSON, D.G., STAMMERJOHN, S.E., IANNUZZI, R.A., SMITH, R.C. & VERNET, M. 2008. Western Antarctic Peninsula physical oceanography and spatio-temporal variability. *Deep-Sea Research II*, **55**, 10.1016/j.dsr2.2008.04.038.

MEHRBACH, C., CULBERSON, C.H., HAWLEY, J.E. & PYTKOWICZ, R.M. 1973. Measurement of the apparent dissociation constants of carbonic acid in seawater at atmospheric pressure. *Limnology and Oceanography*, **18**, 897–907.

MEREDITH, M.P., VENABLES, H.J., CLARKE, A., DUCKLOW, H.W., ERICKSON, M., LENG, M.J., *et al.* 2013. The freshwater system west of the Antarctic Peninsula: spatial and temporal changes. *Journal of Climate*, **26**, 10.1175/JCLI-D-25 12-00246.1.

MOJICA PRIETO, F.J. & MILLERO, F.J. 2002. The values of pK1 + pK2 for the dissociation of carbonic acid in seawater. *Geochimica et Cosmochimica Acta*, **66**, 10.1016/S0016-7037(02)00855-4.

OLSEN, A., LANGE, N., KEY, R.M., TANHUA, T., ÁLVAREZ, M., BECKER, S., *et al.* 2019. GLODAPv2.2019 - an update of GLODAPv2. *Earth System Science Data*, **11**, 10.5194/essd-11-1437-2019.

ORR, J.C., FABRY, V.J., AUMONT, O., BOPP, L., DONEY, S.C., FEELY, R.A., *et al.* 2005. Anthropogenic ocean acidification over the twenty-first century and its impact on calcifying organisms. *Nature*, **437**, 10.1038/nature04095.

REDFIELD, A. 1958. The biological control of chemical factors in the environment. *American Scientist*, **3**, 205–221.

RYSGAARD, S., GLUD, R.N., SEJR, M.K., BENDTSEN, J. & CHRISTENSEN, P.B. 2007. Inorganic carbon transport during sea ice growth and decay: a carbon pump in polar seas. *Journal of Geophysical Research*, **112**, 10.1029/2006JC003572.

SARMIENTO, J.L. & GRUBER, N. 2006. *Ocean biogeochemical dynamics*. Princeton, NJ: Princeton University Press.

SCHOFIELD, O., SABA, G., COLEMAN, K., CARVALHO, F., COUTO, N., DUCKLOW, H., *et al.* 2017. Decadal variability in coastal phytoplankton community composition in a changing West Antarctic Peninsula. *Deep-Sea Research I*, **124**, 42–54.

SMITH, D.A., HOFMANN, E.E., KLINCK, J.M. & LASCARA, C.M. 1999. Hydrography and circulation of the West Antarctic Peninsula continental shelf. *Deep-Sea Research I*, **46**, 10.1016/S0967-0637(98)00103-4.

STAMMERJOHN, S.E., MARTINSON, D.G., SMITH, R.C., YUAN, X. & RIND, D. 2008. Trends in Antarctic annual sea ice retreat and advance and their relation to El Niño-Southern Oscillation and Southern Annular Mode variability. *Journal of Geophysical Research*, **113**, 10.1029/2007JC004269.

THIBODEAU, P.S., STEINBERG, D.K., STAMMERJOHN, S.E. & HAURI, C. 2019. Environmental controls on pteropod biogeography along the Western Antarctic Peninsula. *Limnology and Oceanography*, **64**, 10.1002/lno.11041.

TORTELL, P.D., BITTIG, H.C., KÖRTZINGER, A., JONES, E.M. & HOPPEMA, M. 2015. Biological and physical controls on N_2, O_2, and CO_2 distributions in contrasting Southern Ocean surface waters. *Global Biogeochemical Cycles*, **29**, 10.1002/2014GB004975.

TRÉGUER, P., BOWLER, C., MORICEAU, B., DUTKIEWICZ, S., GEHLEN, M., AUMONT, O., *et al.* 2018. Influence of diatom diversity on the ocean biological carbon pump. *Nature Geoscience*, **11**, 27–37.

TRIMBORN, S., HOPPE, C.J., TAYLOR, B.B., BRACHER, A. & HASSLER, C. 2015. Physiological characteristics of open ocean and coastal phytoplankton communities of Western Antarctic Peninsula and Drake Passage waters. *Deep-Sea Research I*, **98**, 115–124.

TYNAN, E., CLARKE, J.S., HUMPHREYS, M.P., RIBAS-RIBAS, M., ESPOSITO, M., RÉROLLE, V.M.C., *et al.* 2016. Physical and biogeochemical controls on the variability in surface pH and calcium carbonate saturation states in the Atlantic sectors of the Arctic and Southern Oceans. *Deep-Sea Research II*, **127**, 10.1016/j.dsr2.2016.01.001.

VAN HEUVEN, S., PIERROT, D., RAE, J., LEWIS, E. & WALLACE, D. 2011. *MATLAB program developed for CO_2 system calculations. ORNL/CDIAC-105b*. Oak Ridge, TN: Carbon Dioxide Information Analysis Center, Oak Ridge National Laboratory, U.S. Department of Energy, 10.3334/CDIAC/otg.CO2SYS.

VAUGHAN, D.G., MARSHALL, G.J., CONNOLLEY, W.M., PARKINSON, C., MULVANEY, R., HODGSON, D.A., *et al.* 2003. Recent rapid regional climate warming on the Antarctic Peninsula. *Climatic Change*, **60**, 10.1023/A:1026021217991.

VENABLES, H.J., CLARKE, A. & MEREDITH, M.P. 2013. Wintertime controls on summer stratification and productivity at the Western Antarctic Peninsula. *Limnology and Oceanography*, **58**, 10.4319/lo.2013.58.3.1035.

VERNET, M., MARTINSON, D., IANNUZZI, R., STAMMERJOHN, S., KOZLOWSKI, W., SINES, K., *et al.* 2008. Primary production within the sea-ice zone west of the Antarctic Peninsula: sea ice, summer mixed layer, and irradiance. *Deep-Sea Research II*, **55**, 10.1016/j.dsr2.2008.05.021.

WOLF-GLADROW, D.A., ZEEBE, R.E., KLAAS, C., KÖRTZINGER, A. & DICKSON, A.G. 2007. Total alkalinity: the explicit conservative expression and its application to biogeochemical processes. *Marine Chemistry*, **106**, 10.1016/j.marchem.2007.01.006.

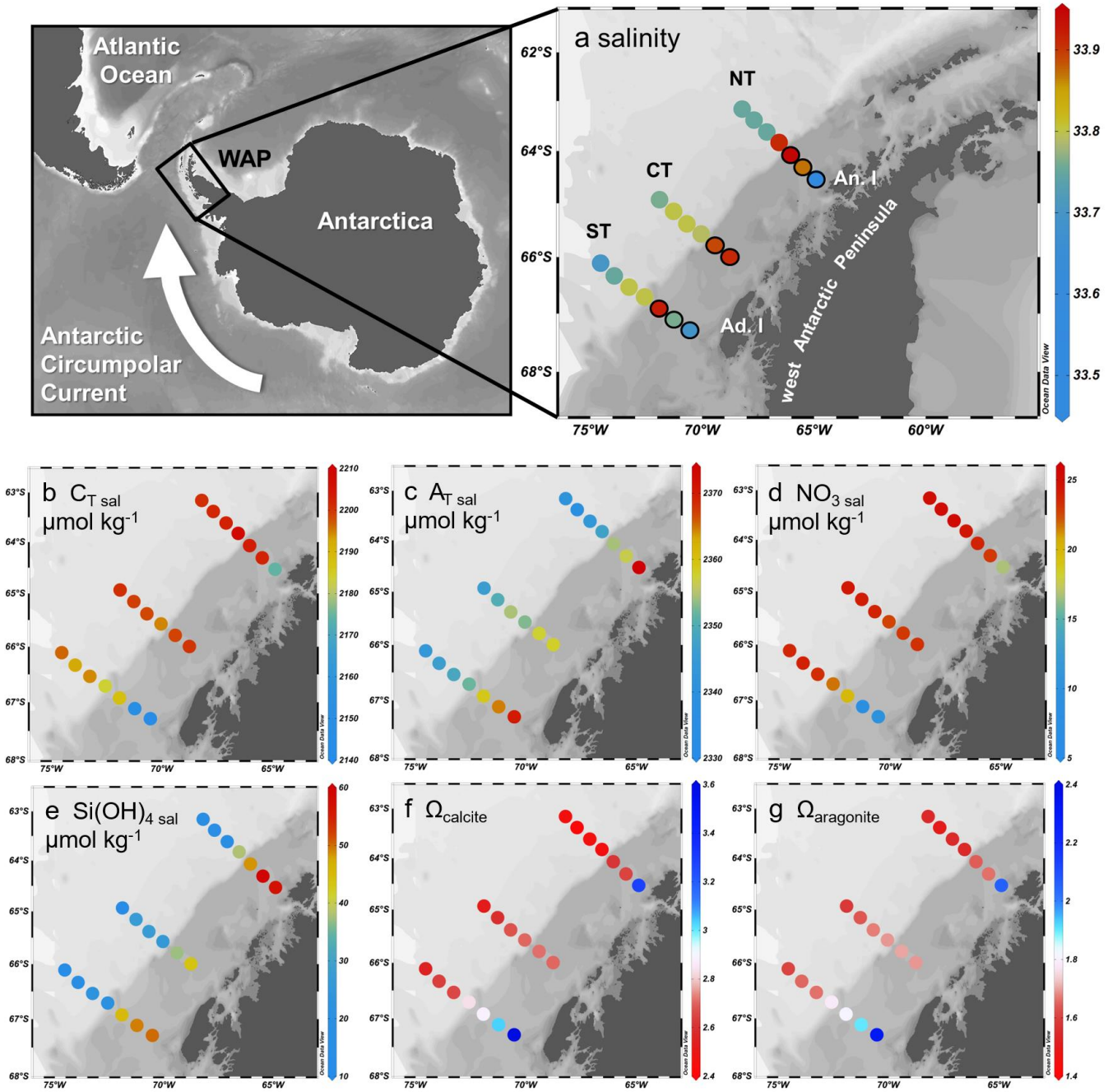

720

721

722 **Fig. 1.** Map of Antarctica and the Southern Ocean showing the West Antarctic Peninsula (WAP) and general direction of flow
723 of the Antarctic Circumpolar Current. Map sub-plots of the WAP showing sea surface **a.** salinity, **b.** salinity-normalized C_T ($C_{T\ sal}$; µmol kg^{-1}), **c.** salinity-normalized $A_{T\ sal}$ ($A_{T\ sal}$; µmol kg^{-1}), **d.** salinity-normalized nitrate ($NO_{3\ sal}$; µmol kg^{-1}), **e.** salinity-
725 normalized silicate ($Si(OH)_{4\ sal}$; µmol kg^{-1}), **f.** calcite saturation state ($\Omega_{calcite}$) and **g.** aragonite saturation state ($\Omega_{aragonite}$). The
726 north (NT), central (CT) and south (ST) transects, shelf stations indicated by black-outlined circles and Anvers Island (An. I)
727 and Adelaide Island (Ad. I) are marked in **a**.

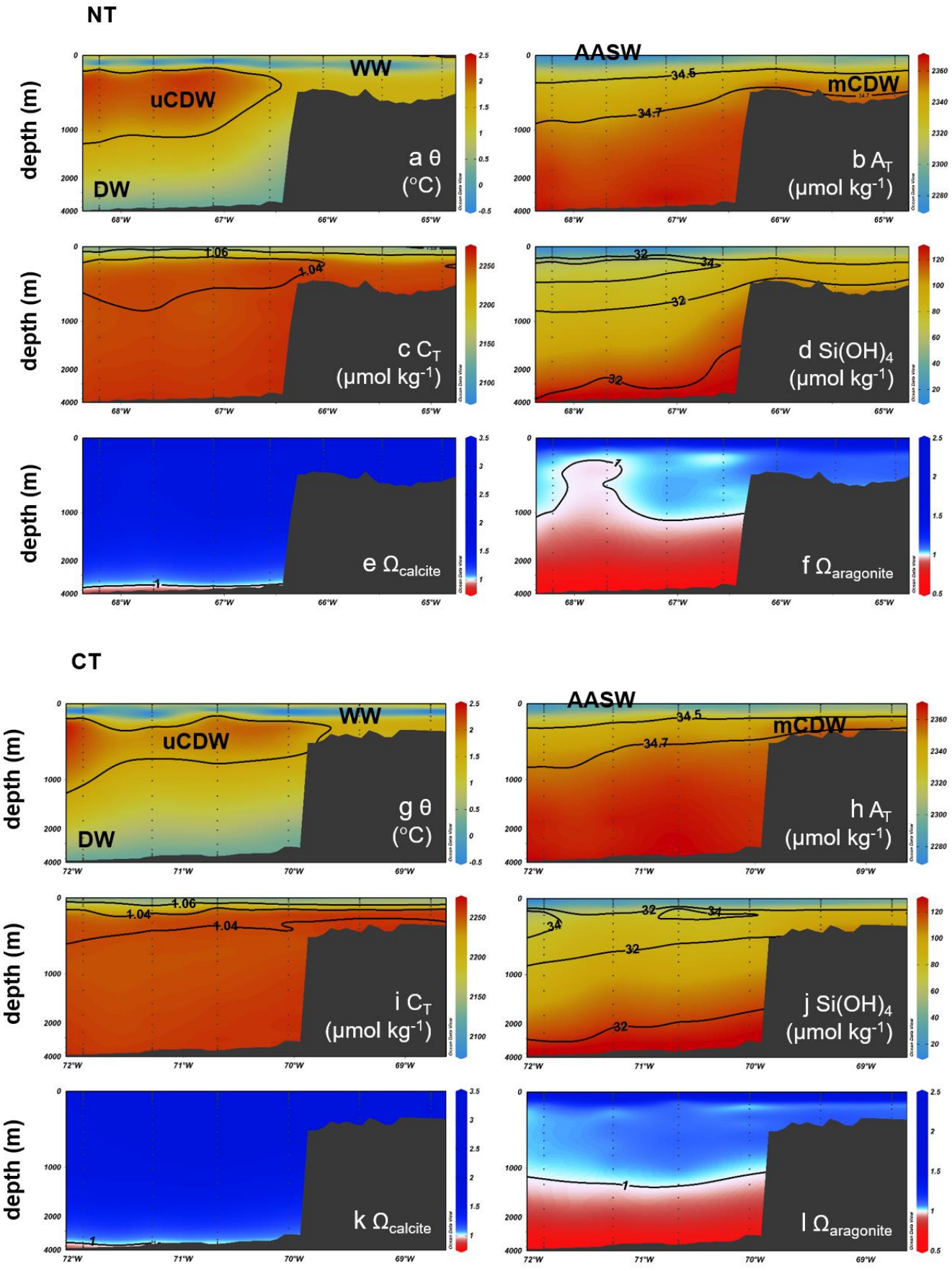
NT
depth (m)
WW
uCDW
DW
a θ (°C)
AASW
mCDW
34.5
34.7
b A_T (μmol kg^{-1})
1.06
1.04
c C_T (μmol kg^{-1})
32
34
d $Si(OH)_4$ (μmol kg^{-1})
e $\Omega_{calcite}$
f $\Omega_{aragonite}$
CT
g θ (°C)
h A_T (μmol kg^{-1})
i C_T (μmol kg^{-1})
j $Si(OH)_4$ (μmol kg^{-1})
k $\Omega_{calcite}$
l $\Omega_{aragonite}$

728

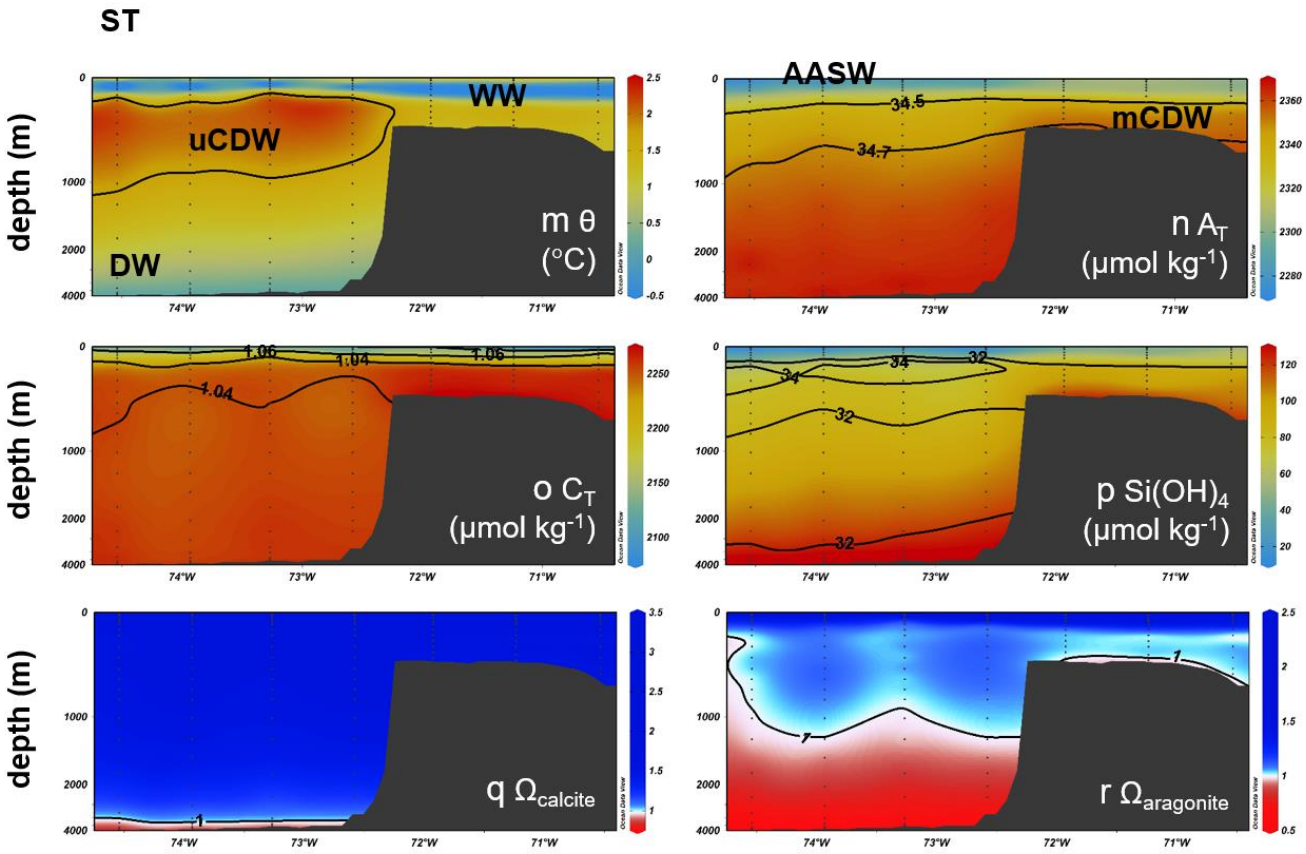

729

730 **Fig. 2.** Vertical distribution along the north (NT; **a.–f.**), central (CT; **g.–l.**) and south (ST; **m.–r.**) transects of (**a.**, **g.**, **m.**) potential
731 temperature (θ, °C), (**b.**, **h.**, **n.**) A_T (µmol kg^{-1}) including salinity contours, (**c.**, **i.**, **o.**) C_T (µmol kg^{-1}) with A_T:C_T ratio contours,
732 (**d.**, **j.**, **p.**) $Si(OH)_4$ (µmol kg^{-1}) with NO_3 (µmol kg^{-1}) contours, (**e.**, **k.**, **q.**) calcite saturation state ($\Omega_{calcite}$) and (**f.**, **l.**, **r.**) aragonite
733 saturation state ($\Omega_{aragonite}$). Boundaries of Antarctic Surface Water (AASW), Winter Water (WW), upper Circumpolar Deep
734 Water (uCDW), modified Circumpolar Deep Water (mCDW) and Deep Water (DW) are indicated. Contours for the calcium
735 carbonate saturation horizon ($\Omega = 1$) are included in **e.**, **f.**, **k.**, **l.**, **q.** and **r**.

736

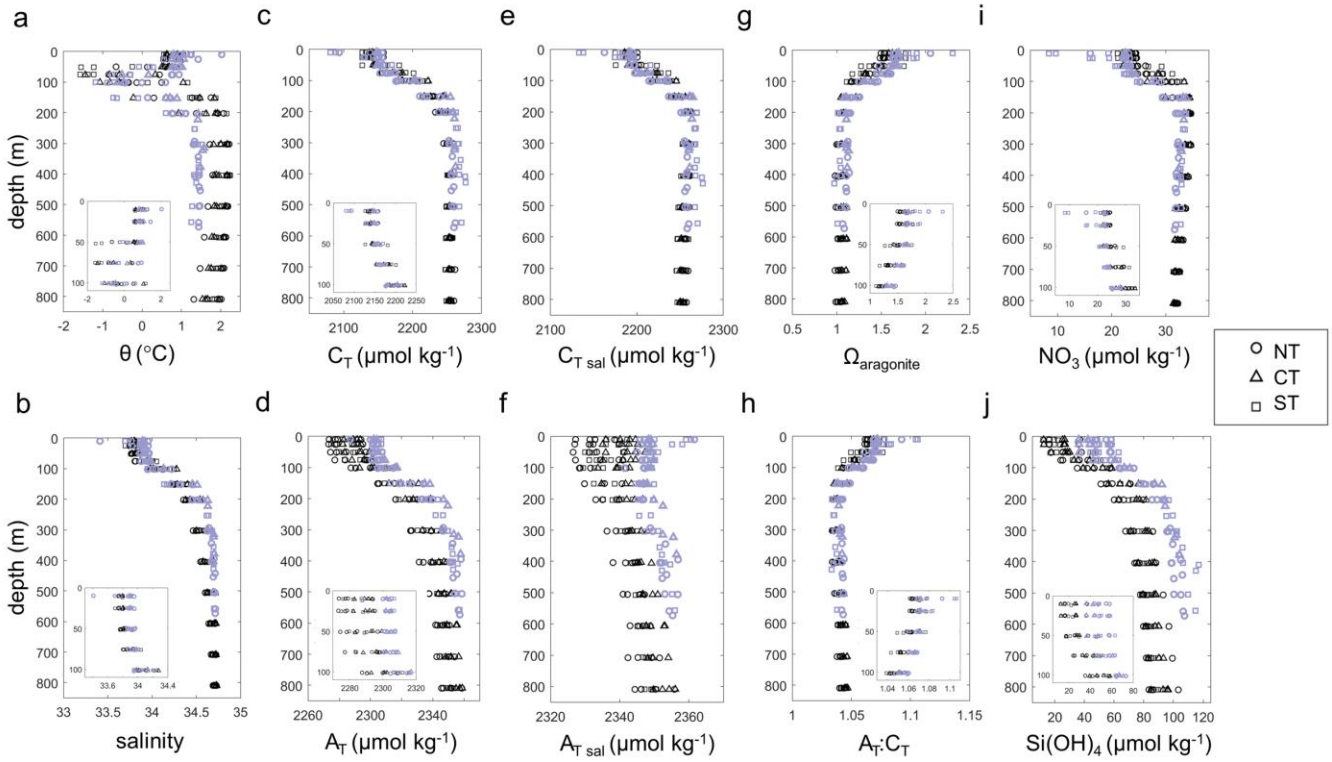

Fig. 3. Vertical profiles of **a.** potential temperature (θ, °C), **b.** salinity, **c.** C_T (µmol kg^{-1}), **d.** A_T (µmol kg^{-1}), **e.** $C_{T\ sal}$ (µmol kg^{-1}), **f.** $A_{T\ sal}$ (µmol kg^{-1}), **g.** aragonite saturation state ($\Omega_{aragonite}$), **h.** the A_T:C_T ratio, **i.** NO_3 (µmol kg^{-1}) and **j.** $Si(OH)_4$ (µmol kg^{-1}) in the upper 850 m (inserts showing upper 120 m) for offshore (black symbols) and shelf (blue symbols) for the north (NT, circles), central (CT, triangles) and south (ST, squares) transects.

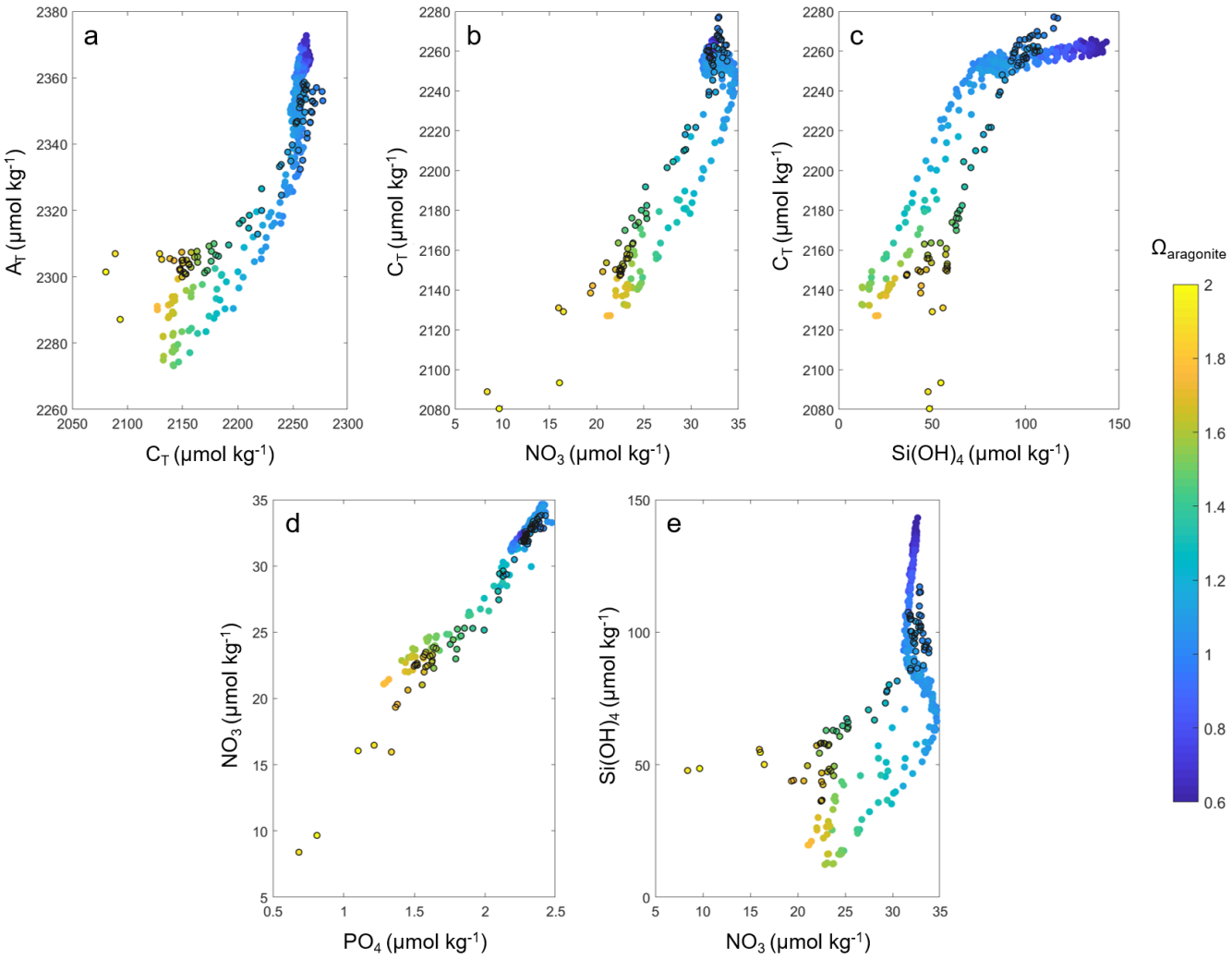

743

744 **Fig. 4.** Relationships between **a.** A_T (µmol kg^{-1}) and C_T (µmol kg^{-1}), **b.** C_T (µmol kg^{-1}) and NO_3 (µmol kg^{-1}), **c.** C_T (µmol kg^{-1})
745 and $Si(OH)_4$ (µmol kg^{-1}), **d.** NO_3 (µmol kg^{-1}) and PO_4 (µmol kg^{-1}) and **e.** $Si(OH)_4$ (µmol kg^{-1}) and NO_3 (µmol kg^{-1}). Data are
746 colour coded with respect to the aragonite saturation state ($\Omega_{aragonite}$) and shelf waters are identified by black-outlined circles.

747

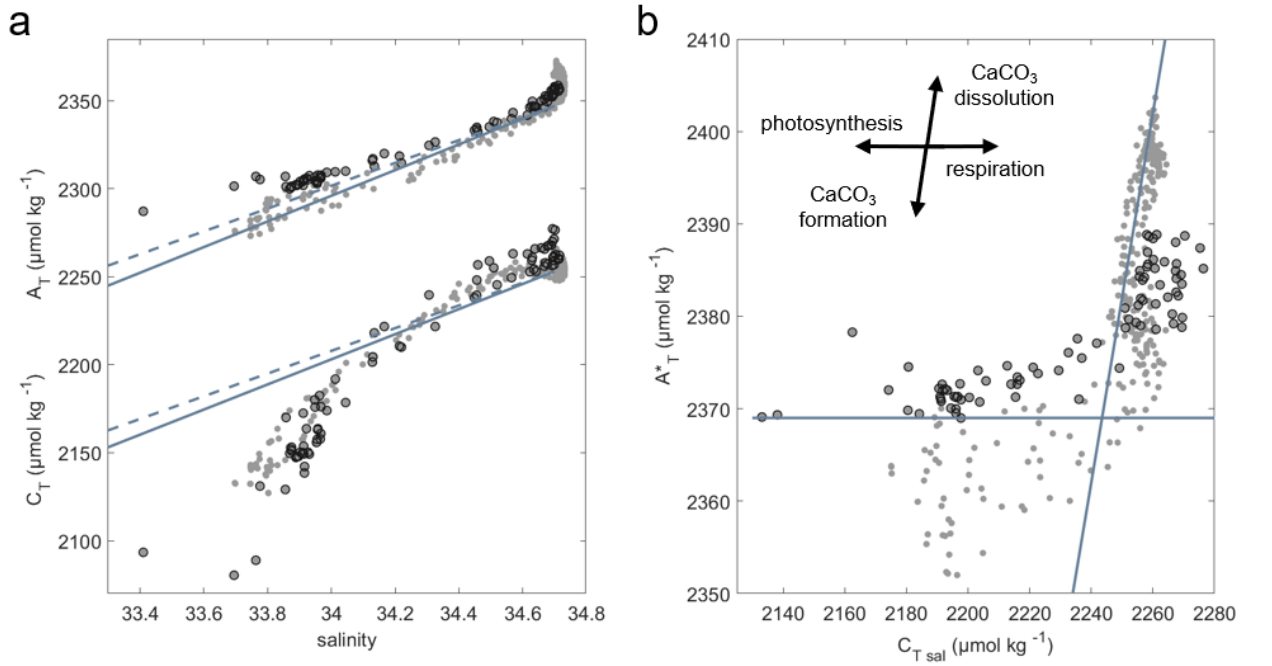

748

749 **Fig. 5.** Relationships between **a.** salinity and A_T (µmol kg^{-1}) and salinity and C_T (µmol kg^{-1}), and **b.** potential A_T (A_T*; µmol kg^{-1}) and salinity-normalized C_T ($C_{T\ sal}$; µmol kg^{-1}) for all data (grey dots) and the seasonal mixed layer (Antarctic Surface Water
750 and Winter Water, black-outlined circles). Trend lines in **a.** represent the hypothetical dilution lines between endmembers for
751 upper Circumpolar Deep Water with glacial ice (dashed lines) and sea ice (solid lines). Trend lines in **b.** represent the influence
752 of photosynthesis/respiration and carbonate mineral formation/dissolution, as indicated by the insert.

753

754

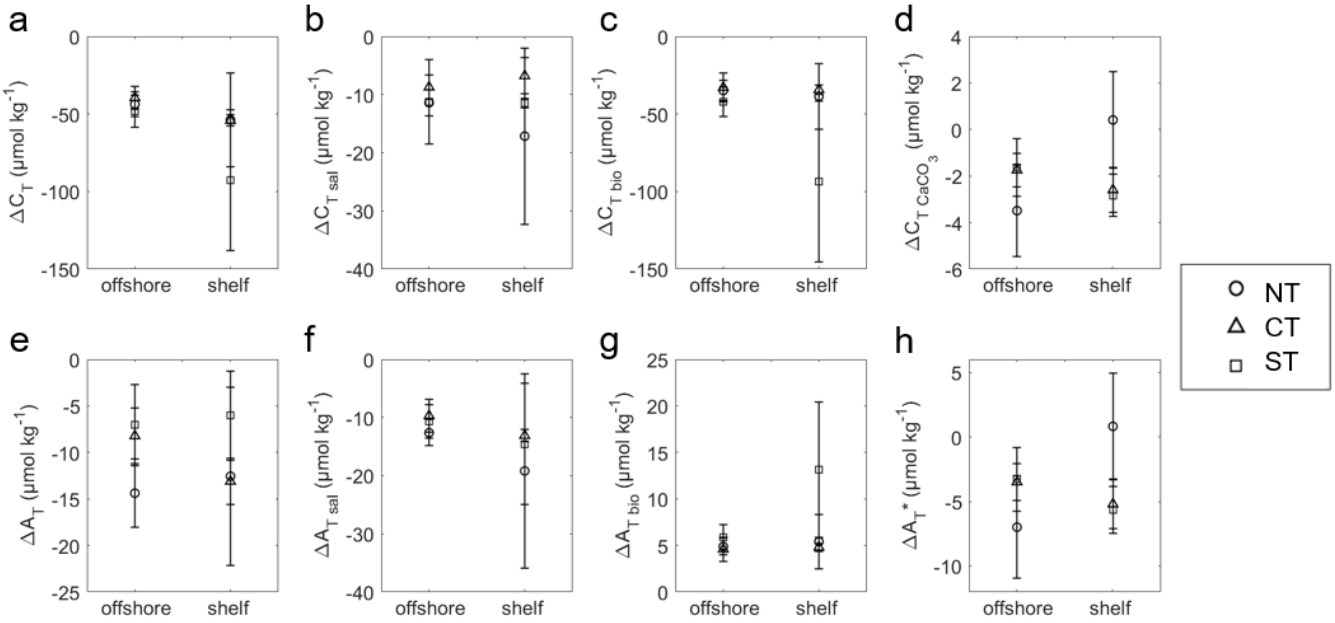

755

Fig. 6. Deficits in C_T and A_T between the summer mixed layer and Winter Water ascribed to: (**a.**, **e.**) total change in C_T (ΔC_T; µmol kg^{-1}) and total change in A_T (ΔA_T; µmol kg^{-1}); (**b.**, **f.**) changes due to salinity ($\Delta C_{T\ sal}$, $\Delta A_{T\ sal}$; µmol kg^{-1}); (**c.**, **g.**) changes due to photosynthesis/respiration ($\Delta C_{T\ org}$, $\Delta A_{T\ org}$; µmol kg^{-1}); and (**d.**, **h.**) changes due to calcium carbonate mineral formation/dissolution ($\Delta C_{T\ CaCO3}$, ΔA_T*; µmol kg^{-1}). Mean values with error bars (± 1 SD) are shown for offshore and shelf waters for the north (NT, circles), central (CT, triangles) and south (ST, squares) transect.

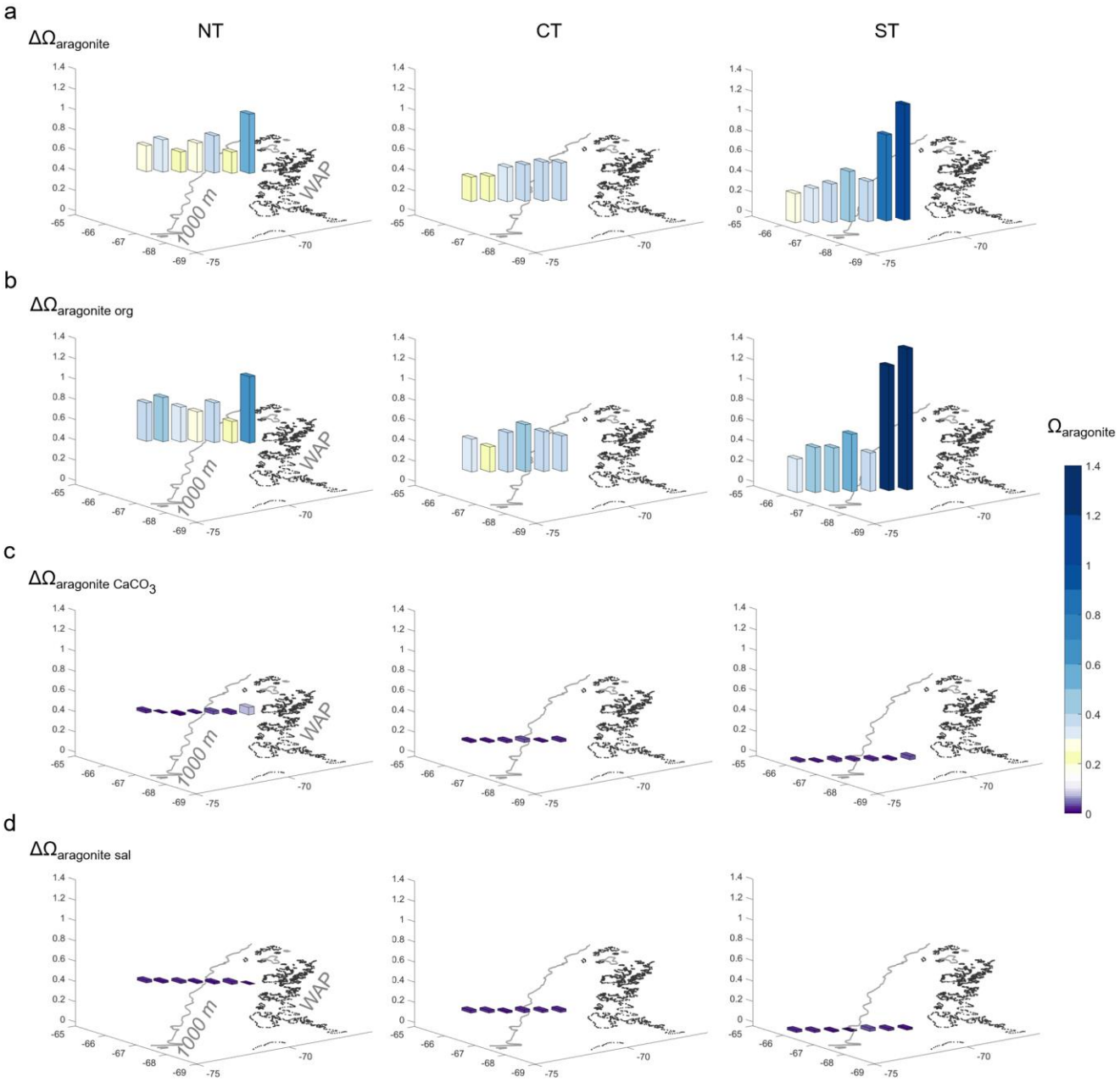

Fig. 7. Changes in the aragonite saturation state ($\Omega_{aragonite}$) between the summer mixed layer and Winter Water along the West Antarctic Peninsula ascribed to **a.** the total change ($\Delta\Omega_{aragonite}$), **b.** changes due to photosynthesis/respiration ($\Delta\Omega_{aragonite\ org}$), **c.**

765 changes due to the formation/dissolution of any calcium carbonate minerals ($\Delta\Omega_{aragonite\ CaCO3}$) and **d.** changes due to salinity
766 ($\Delta\Omega_{aragonite\ sal}$) for each hydrographic station in the north transect (NT), central transect (CT) and south transect (ST). Uncertainties
767 are $\Delta\Omega_{aragonite\ sal} \pm 0.29$, $\Delta\Omega_{aragonite\ org} \pm 0.05$ and $\Delta\Omega_{aragonite\ CaCO3} \pm 0.41$ (not taken into account is the ± 0.04 uncertainty in $\Omega_{aragonite}$
768 from the use of different equilibrium constants K_1 and K_2).

769

770 **Table I.** Water mass classification and inorganic carbon system parameters C_T (μmol kg^{-1}), A_T (μmol kg^{-1}), calcite saturation
771 state ($\Omega_{calcite}$) and aragonite saturation state ($\Omega_{aragonite}$) along the north transect (NT), central transect (CT) and south transect (ST)
772 for Antarctic Surface Water (AASW), Winter Water (WW), upper Circumpolar Deep Water (uCDW), modified Circumpolar
773 Deep Water (mCDW) and Deep Water (DW). Average values are shown per water mass per transect with the (±) standard
774 deviation in parentheses.

Water mass		Transect	C_T (μmol kg^{-1})		A_T (μmol kg^{-1})		$\Omega_{calcite}$		$\Omega_{aragonite}$	
			Offshore	Shelf	Offshore	Shelf	Offshore	Shelf	Offshore	Shelf
AASW	$\sigma_0 \leq 27.4$	NT	2150 (9)	2150 (18)	2283 (9)	2302 (5)	2.38 (0.08)	2.65 (0.21)	1.49 (0.05)	1.66 (0.13)
		CT	2145 (8)	2154 (10)	2292 (6)	2305 (3)	2.58 (0.11)	2.63 (0.12)	1.62 (0.07)	1.65 (0.07)
		ST	2136 (11)	2144 (31)	2284 (6)	2305 (2)	2.60 (0.20)	2.78 (0.48)	1.63 (0.12)	1.74 (0.30)
WW	θ_{min}	NT	2190 (13)	2188 (19)	2296 (9)	2310 (5)	1.99 (0.11)	2.20 (0.19)	1.25 (0.07)	1.38 (0.12)
	$\sigma_0 \leq 27.2$–27.4	CT	2181 (5)	2203 (2)	2298 (7)	2317 (1)	2.13 (0.05)	2.09 (0.02)	1.34 (0.03)	1.31 (0.01)
		ST	2181 (8)	2197 (18)	2291 (6)	2310 (3)	2.05 (0.03)	2.06 (0.20)	1.29 (0.02)	1.29 (0.13)
uCDW	$1.70 \leq \theta_{max} \leq 2.13$°C[a]	NT	2255 (2)	-	2347 (5)	-	1.60 (0.05)	-	1.02 (0.03)	-
		CT	2254 (2)	-	2348 (5)	-	1.71 (0.05)	-	1.08 (0.03)	-
	$34.54 \leq S \leq 34.75$[a]	ST	2252 (3)	-	2347 (4)	-	1.68 (0.07)	-	1.07 (0.04)	-
	< 2000 m									
mCDW	$34.6 \leq S \leq 34.7$[b]	NT	-	2253 (1)	-	2347 (0)	-	1.77 (0.01)	-	1.12 (0.00)
		CT	-	2261 (1)	-	2353 (5)	-	1.77 (0.02)	-	1.11 (0.01)
	< 750 m	ST	-	2270 (5)	-	2352 (5)	-	1.62 (0.04)	-	1.02 (0.03)
DW	$34.7 \leq S_{max}$	NT	2262 (2)	-	2366 (2)	-	1.01 (0.12)	-	0.66 (0.07)	-
		CT	2261 (2)	-	2369 (2)	-	1.08 (0.12)	-	0.70 (0.08)	-
	> 2000 m[c]	ST	2261 (3)	-	2366 (1)	-	0.99 (0.15)	-	0.65 (0.09)	-

[a]Martinson *et al.* (2008).

[b]Smith *et al.* (1999).

[c]Hauri *et al.* (2015).

'-' indicates no data.